
Article:

Chen, Y.-T., Sui, J., Yang, Y. et al. (2025) Integration of gut microbiome and lipid metabolism reveals the anti-cancer effects of pentadecanoic acid on bladder cancer. BMC Medicine, 24 (10). ISSN: 1741-7015

https://doi.org/10.1186/s12916-025-04554-5

Chen *et al. BMC Medicine* (2026) 24:10
https://doi.org/10.1186/s12916-025-04554-5

BMC Medicine

RESEARCH **Open Access**

Integration of gut microbiome and lipid metabolism reveals the anti-cancer effects of pentadecanoic acid on bladder cancer

Ya-Ting Chen[1,2†], Jing Sui[1,3†], Yu Yang[1,4†], Hao Zhang[5†], Anke Wesselius[6], Yingzhou Shen[7], Qi-Rong Qin[8,9,10], Gui-Ju Sun[1,4], Shao-Kang Wang[1,4], Xiang-Dong Wang[11,12], Shujin Wang[13], Wen-Chao Li[14], Kar Keung Cheng[15], Nicholas D. James[16,17], Richard T. Bryan[16], Maurice P. Zeegers[6], Lianmin Chen[18,19*], Hui Xia[1,4*] and Evan Yi-Wen Yu[1,2,6*]

Abstract

Background Pentadecanoic acid (PEA), an odd-chain fatty acid derived from diet by the gut microbiome, has garnered increasing attention for its systemic health-promoting properties. Its potential role in bladder cancer (BC) occurrence and invasion, however, remains unclear.

Methods Large-scale cohorts' analyses were performed to assess the association between dietary PEA and BC occurrence and invasion. In vitro and in vivo experiments, including EJ and T24 BC cell assays and a BBN-induced mouse model, were conducted to experimentally assess the impact of PEA on BC. Serum proteomics, gut microbiome, and targeted fecal lipidomics analyses were employed to explore the underlying mechanisms.

Results Dietary PEA was negatively associated with BC occurrence and invasion in cohort analyses. PEA suppressed EJ and T24 BC cell migration, invasion, and proliferation, while inhibiting BC development in a BBN-induced mouse model. In vivo serum proteomics identified differentially expressed lipid-related proteins (e.g., Apoe and Apob) following PEA treatment, implicating its modulation of lipid metabolism pathways. Considering the essential role of the *gut-bladder* axis, the gut microbiome analysis exhibited that PEA markedly altered bacteria (e.g., g_*Alistipes*) and fungi (e.g., o_*Erysiphales*, g_*Teberdinia*, and g_*Gibberella*), with concomitant lipid metabolism changes. Furthermore, targeted fecal lipidomics demonstrated the shifts in key lipids, such as phosphatidylethanolamines (PE) involved in essential lipid clusters, suggesting regulation by gut microbiome linked to BC development.

Conclusions Collectively, our findings demonstrate that PEA mitigates BC by reshaping the gut microbiome and modulating lipid metabolism, providing new insights into its molecular and therapeutic potential.

Keywords Bladder cancer, Pentadecanoic acid, Gut microbiome, Lipid metabolism, Gut-bladder axis

---

† Ya-Ting Chen, Jing Sui, Yu Yang and Hao Zhang contributed equally to this work.

*Correspondence:
Lianmin Chen
lianminchen@njmu.edu.cn
Hui Xia
huixia@seu.edu.cn
Evan Yi-Wen Yu
evan.yu@maastrichtuniversity.nl
Full list of author information is available at the end of the article

Graphical Abstract

This study aims to investigate the effects of PEA on BC occurrence and invasion using multi-dimensional approaches. We found PEA showing the protective effect on BC based on large-scale cohorts, in vitro and in vivo experiments. This observation may be mediated by the gut microbiome's involvement in the lipid-metabolism pathway, potentially highlighting a *gut-bladder* axis in BC. Abbreviations: PEA, pentadecanoic acid; BC, bladder cancer; BCPP, Bladder Cancer Prognosis Programme; CCK-8, Cell Counting Kit-8; DIA MS, Data-Independent Acquisition Mass Spectrometry; 16S rRNA, 16S ribosomal RNA; ITS, Internal Transcribed Spacer; LC-MS/MS, Liquid Chromatography-Tandem Mass Spectrometry; PE, phosphatidylethanolamine.

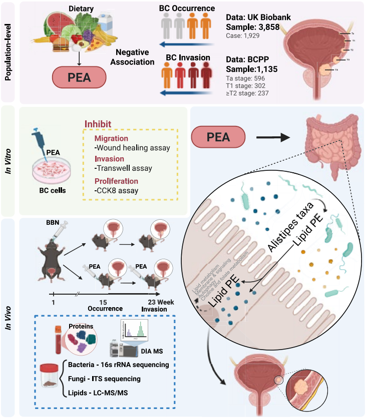

Background

Pentadecanoic acid (PEA), an odd-chain fatty acid (OCFA), has been progressively emphasized for its potential benefits to human health [1]. PEA is predominantly found in dairy and ruminant meat rather than being synthesized endogenously, comprising approximately 0.89% of total fatty acids [2], and is widely recognized as a biomarker of dairy fat intake [1, 3]. Accumulating evidence has demonstrated that dietary PEA is linked to a lower risk of various diseases [4–15], including certain cancers [16–18]. Notably, a daily intake of 200 to 300 mg of PEA is considered potentially beneficial, further highlighting its relevance to human health [1, 19]. However, current evidence regarding its anti-cancer effects remains limited.

Bladder cancer (BC), one of the most common malignancies, has been reported to be influenced by dietary factors, given that circulating dietary compounds—such as OCFAs—come into direct contact with the bladder epithelium [20]. A prior study has reported that higher circulating levels of OCFAs (specifically, PEA and heptadecanoic acid) associated with a lower risk of BC [18]. In line with this, we also identified that OCFAs (specifically, PEA and nonanoic acid) negatively associated with BC invasion [21]. However, those findings were population-based, while the underlying mechanisms remain largely unexplored.

PEA has been reported to exert anti-inflammatory, anti-fibrotic, and anti-cancer effects, potentially through the activation of AMPK and PPAR-α/δ pathways, and the inhibition of mTOR, JAK-STAT, and HDAC6 signaling [22–27]. In addition, its anti-microbial properties may modulate the composition and diversity of the gut microbiome, including both bacterial and fungal communities, which could further contribute to its biological effects [28, 29]. According to Wei et al., gut microbiome-derived short-chain fatty acids (SCFAs) exhibit anti-inflammatory properties and that inulin supplementation enriches PEA-related gut bacteria, thereby restoring intestinal barrier integrity and alleviating diet-induced nonalcoholic steatohepatitis (NASH) in mice [15].

The gut microbiome, comprising diverse bacterial and fungal communities, plays a pivotal role in regulating host metabolism, immune responses, and inflammation—key processes in cancer development [30–33]. Given PEA's potential to modulate the microbiome, it may enhance the production of beneficial metabolites that mediate its anti-cancer effects [34]. However, the role of the gut microbiome—including both bacteria and fungi—and its crosstalk with extraintestinal diseases such as BC remains poorly understood, particularly in the context of the *gut-bladder* axis, which has long been overlooked [35]. Therefore, elucidating how dietary PEA shapes the gut microbiome is critical for understanding its systemic effects on cancer.

Hence, in this study, we aimed to investigate the effect of PEA and its potential mechanisms, focusing on *gut-to-bladder* regulation by integrating population investigation coupled with in vitro and in vivo experiments, in protecting against BC.

Methods

Population-level study design

Study population

This study is reported as per the STROBE guideline (refer to Additional file 1: STROBE checklist). We leveraged data from two cohorts, i.e., UK Biobank and Bladder Cancer Prognosis Programme (BCPP), to investigate the association of dietary PEA with BC occurrence and invasion, respectively.

A detailed description of the UK Biobank cohort, including study populations and data collection, has been previously described elsewhere [36]. The UK Biobank database for this project initially included 502,505 participants under Application #55889. Exclusion criteria included the withdrawal of informed consent ($n=12$), incomplete information prevalent BC cases at baseline ($n=2,420$), and missingness on smoking status ($n=2,049$). To balance the disparity between BC cases and non-BC controls in the UK Biobank, an exact 1:1 matching method was used. Each BC case was matched with a non-BC control based on age, sex, and smoking status. Finally, 3,858 individuals (including 1,929 BC cases) were eligible for the current analyses.

The BCPP is a multicenter epidemiological prospective cohort study with 1,550 participants recruited from 10 different hospitals in the West Midlands. Details of the cohort have been published previously [37]. The aim of the BCPP is to gather information on the determinants of BC and its prognosis. Participants were eligible for cystoscopy findings that were suggestive of BC. Case report forms contained data on tumor characteristics, initial treatment, and event data, including recurrences. The study protocol was approved by the Nottingham Research Ethics Committee (06/MRE04/65), and written informed consent was obtained from all participants. Exclusion criteria included the withdrawal of informed consent ($n=20$), missing stage data ($n=249$), and missingness on smoking status ($n=122$). In addition, TX (primary tumor cannot be assessed) and T0 (no evidence of primary tumor) cases ($n=10$) were excluded due to lack of histopathological confirmation, as they represented either unassessable primary tumors or benign lesions that had spontaneously regressed. Furthermore, Tis ($n=14$) were also excluded due to the limited sample size. Finally, 1,135 individuals were eligible for the current analyses.

Occurrence and invasion of BC ascertainment

In the UK Biobank, the definitions for BC cases were restricted with an International Classification of Diseases (ICD) codes of C67.0, C67.1, C67.2, C67.3, C67.4, C67.5, C67.6, C67.7, C67.8, C67.9, D09.0 (ICD10) and 1880, 1881, 1882, 1883, 1884, 1885, 1886, 1887, 1888, 1889, 2337 (ICD9); and self-report/doctor-diagnosis (code 1035 in field 20001). To prevent bias from analyzing heterogeneous molecular BC subtypes, histology was limited to the following ICD Oncology codes: 8000 (neoplasm), 8001 (tumor cells), 8010 (carcinoma), 8020 (carcinoma, undifferentiated), 8050 (papillary carcinoma), 8120 (transitional cell carcinoma), and 8130 (papillary transitional cell carcinoma).

In the BCPP, BC invasion was defined based on the UICC staging system, specifically using the T category, which describes the extent of tumor invasion into the bladder wall [37]. The staging system categorizes BC with classifications ranging from TX (primary tumor cannot be assessed) and T0 (no evidence of primary tumor) to Ta (non-invasive papillary carcinoma), Tis (carcinoma in situ), T1 (tumor invades the subepithelial connective tissue), T2 (tumor invades the muscle layer), T3 (tumor invades the perivesical fatty tissue), and T4 (tumor invades surrounding structures like the prostate, uterus, vagina, pelvic wall, or abdominal wall).

Dietary PEA assessment

In the UK Biobank, the initial 502,505 participants were invited to provide information on their food intake in the past year through a touch questionnaire at the assessment centers [36]. The food frequency questionnaire (FFQ) (Category 100052), which contains data from the touchscreen questionnaire on the reported frequency of intake of a range of common food and drink items, was used to calculate the intake of PEA from dietary. In the BCPP, all data were collected prospectively. Baseline data collection was done using a semi-structured questionnaire administered by research nurses before initial treatment for BC. This questionnaire collected information concerning sociodemographic data, medical history, environmental exposures, use of medications, diet, smoking behavior, health-related quality of life, and social support. Since the main sources of PEA are dairy products and animal fats [38], the milk intake from the FFQ outside the food questionnaire was also included in the analysis. Participants were asked "how often on average you have eaten each of the food types that are listed during the past year (never or less than once per month,1–3 per month, once per week, 2–4 per week, 5–6 per week, and at least once per day)".

The food intake (g/week) was extracted as the representative intake by multiplying the daily intake portions with the consumed amounts according to the Maff Handbook [39]. The PEA content for each food (i.e., the amount of PEA per 100 g of food) is the average value of the PEA content for that type of food recorded in the Composition of Foods Integrated Dataset (CoFID) [40]. Then, the intake of PEA from dietary (g/week) was calculated based on the amount of PEA per 100 g of food (refer to Additional file 2: Table S1). Before the analysis, dietary PEA was standardized to facilitate better interpretation of the results.

Covariates ascertainment and statistical analysis

A set of covariates, i.e., age (years; continuous), sex (males or females), smoking status (never, former, and current), body mass index (BMI; kg/m^2; continuous), ethnicity (white, non-white, or prefer not to answer), household income (average total household income before tax; categorical), and educational qualification (categorical) was selected based on their potential confounding effect as indicated in the literature concerning the association with both the exposure (i.e., PEA) and outcome (i.e., BC occurrence and invasion). These covariates were derived from the baseline general questionnaire.

Descriptive statistics are presented as mean [standard deviation (SD); normally distributed continuous variables] or median (interquartile range; skewed distribution) for continuous variables and frequency (percentage, %) for categorical variables. The participants were categorized into 2 groups according to the BC occurrence (i.e., BC case and non-BC control) in the UK Biobank and categorized into 3 groups according to the BC invasion (i.e., Ta, T1, and ≥ T2) in BCPP. The differences in characteristics of participants in the groups were tested using an ANOVA test for continuous variables and a chi-square (χ^2) test for categorical variables. The mean intake (g/week) of PEA was depicted across the groups.

The assessment of dietary PEA and BC was conducted separately for the UK Biobank and the BCPP. To assess the association between dietary PEA and BC occurrence in the UK Biobank, binomial logistic regression analysis was performed. The associations were assessed using three models; model 1: without covariate adjustment, as the data had already been fully matched for age, sex, and smoking status; model 2: adjusted for BMI; model 3: additionally adjusted for qualification, household income, and ethnicity. For evaluating the association between dietary PEA and BC invasion in the BCPP, ordered multinomial logistic regression analysis was used, assuming proportionality. The associations were assessed applying three models; model 1: crude model without adjustment; model 2: adjusted for sex, age, and smoking status; model 3: additionally adjusted for ethnicity. We also conducted a sensitivity analysis by categorizing BC into non-muscle invasive BC (NMIBC, including Ta, T1) and muscle-invasive BC (MIBC, including T2 and above) to analyze the association with dietary PEA using binomial logistic regression. The results were also presented as ORs with 95% CIs.

The statistical analyses were performed using STATA version 14 SE (Stata Corporation, TX, USA), and R software (version 4.1.1, free software, see https://www.r-project.org/foundation/). A two-tailed $p < 0.05$ was considered significant.

In vitro experiments design

The human BC cells EJ (EJ-1) (provided by Zhongda Hospital affiliated with Southeast University) and T24 (purchased from Guangzhou Kinlogix Biotechnology Co., Ltd.) were used in study. EJ BC cell were cultured in Roswell Park Memorial Institute 1640 Medium (RPMI 1640) supplemented with 10% fetal bovine serum (FBS), while T24 cell were cultured in Dulbecco's modified Eagle's medium (DMEM) supplemented with 10% FBS. Treatment PEA was purchased from MedChemExpress (MCE). Cells were treated with PEA at 200 μmol/L, dissolved in dimethyl sulfoxide (DMSO). Cells in control group were treated with an equivalent volume of DMSO. To evaluate the effects of PEA on BC cell proliferation and migration, wound healing, transwell, and Cell Counting Kit-8 (CCK-8) assays were performed. The wound healing assay and transwell assay were conducted with reference to a previous study [41].

Wound healing assay

EJ and T24 BC cells were seeded in six-well plates at a density of 5×10^5 cells/well and incubated for 24 h. Following washing with PBS, sterile pipette tips were used to make a straight scratch, removing the cells from the scratched area. Then, the remaining cells were treated with PEA, with DMSO serving as the control. Images were captured at 0 h, 24 h, 48 h, and 72 h using an inverted microscope, and the width of the scratch was measured. The migration closure was calculated by subtracting the scratch width at each time point from the initial scratch width, dividing by the initial width, and multiplying by 100.

Transwell assay

EJ and T24 BC cells were seeded in the upper chamber of a 6-well transwell plate at a density of 2×10^5 cells/well. 1.5 mL of serum-free medium was added to the upper chamber, and 2 mL of complete medium containing 10% FBS was placed in the lower chamber. PEA was added to the upper chamber, with DMSO serving as the control. The plates were then incubated for 48 h at 37 °C, 5% CO^2. After rinsing with PBS, the cells on the membrane were fixed with paraformaldehyde and then stained with 0.1% crystal violet. Non-migrated cells on the upper side of the membrane were gently wiped off with a cotton swab. After washing the membrane three times with PBS, the migrated cells were observed under the microscope. Random fields were taken for counting, and the average number of migrated cells was quantified to assess cell migration.

CCK-8 assay

EJ and T24 BC cells were seeded in 96-well plates at a density of 2×10^3 cells/well, and each group had 5 replicates. After culturing the cells in the incubator for 24, 48, and 72 h, the old medium was discarded, and 10 μL of CCK-8 reagent was added to each well, followed by 100 μL of complete medium. The cells were then incubated for an additional 1 h. The absorbance at 450 nm was measured using an ELISA reader. Cell viability was used as an indicator of cell proliferation. The viability of the control group was defined as 100%, and the relative viability of each group was calculated using the formula: (OD_{450} of treatment group/OD_{450} of control group) × 100.

In vivo experiments design

This study is reported as per the ARRIVE guideline (refer to Additional file 3: ARRIVE checklist). The animal experimental protocols were approved by the Animal Ethical Council of Southeast University and were executed in compliance with the National Guidelines for Experimental Animal Welfare. All efforts were made to minimize the suffering of animals. Male C57BL/6 mice, aged 4–5 weeks, were obtained from a certified animal breeding facility. All mice were housed in a controlled environment with a 12 h light/dark cycle, constant temperature (22 ± 2 °C), and humidity (55 ± 5%). They were provided with standard laboratory chow and water ad libitum. All experimental procedures were conducted in accordance with institutional guidelines and approved by the Animal Care and Use Committee. To induce BC, N-butyl-N-(4-hydroxybutyl) nitrosamine (BBN) was administered by oral gavage (in 0.2 mL of 20% ethanol) to each mouse every other day for 12 weeks. A total of 80 mice was randomly allocated and divided into 4 groups comprising 20 mice for each: control group, BC model group, low-dose PEA-treated group with BBN-induced group (BC PEAL), and high-dose PEA-treated group with BBN-induced group (BC PEAH). Randomization was performed using R software, with animals stratified by body weight to ensure balanced allocation across experimental groups. The sample size calculation was performed using online software (https://select-statistics.co.uk/calculators/), with the power set to 80%, requiring 7 mice per group, and 10 mice per group were set to account for potential losses. Throughout the study, mice were monitored for body weight changes every 2 weeks, and for their overall health status. Except for one mouse in the control group at the invasion stage, which was excluded due to poor health, all other groups consisted of 10 mice each.

PEA administration

Groups included BC PEAL and BC PEAH started receiving PEA via daily oral gavage 1 week before BBN administration. The administration of PEA was maintained throughout the entire experimental period, with BC PEAL receiving 35 mg/kg and BC PEAH receiving 350 mg/kg.

Specimen collection

At week 15, 10 mice from each group were euthanized to observe the onset of BC. At week 23, an additional 10 mice from each group were euthanized to observe the invasion of BC simultaneously. Tissue samples, fecal samples, blood, and other relevant specimens were collected from all mice for subsequent analysis.

Histological, proteomics, gut microbiome, and targeted lipidomic analyses were performed to evaluate tissue characteristics and molecular alterations in vivo.

Histological analysis

Tissue samples from the bladder were fixed in neutral buffered formalin, embedded in paraffin, and sectioned for histological examination. Following embedding, sections were baked at 80–90 °C for 20 min before undergoing hematoxylin and eosin (H&E) staining. Deparaffinization and hydration of the paraffin sections were performed, followed by hematoxylin staining for 5–10 min, rinsing in running water for 5 min, differentiation in hydrochloric acid–ethanol for 3 s, and bluing in running water for 30 min. Eosin staining was then performed for 1–2 min, followed by rinsing to remove excess stain. Sections were dehydrated through a graded ethanol series, cleared in xylene, and mounted with neutral resin.

Additionally, immunohistochemical staining for Ki-67 was conducted to assess cell proliferation, providing critical information regarding tumor growth and invasion. The sections were deparaffinized with xylene and hydrated through a graded ethanol series to water. Antigen retrieval was performed using a 50-fold concentrated citrate buffer in a microwave at 800 W for 15 min, followed by cooling to room temperature and rinsing with distilled water twice. Sections were then incubated in a solution containing 3% H_2O_2 for 10 min to eliminate endogenous peroxidase activity. After washing, the area of interest was circled using an immunohistochemical pen. The primary antibody (1:200) was diluted in PBS and incubated overnight at 4 °C. After three washes with PBS, the secondary antibody (1:1000) was diluted in PBS and incubated at 37 °C for 35 min, followed by three additional washes with PBS. The sections were developed with DAB for 2 min, counterstained with hematoxylin for 30 s, rinsed twice in running water, differentiated for 2 s, and then rinsed again twice in running water. Finally, the sections were treated with warm water for 10 min to achieve bluing, completing the dehydration, clearing, and mounting processes.

All sections were analyzed using a blind method by experienced researchers and specially trained pathologists to ensure objectivity and accuracy in the results.

Proteomics analysis

Serum proteins were extracted from blood samples using the TioMagnTM Plus serum/plasma low-abundance enrichment kit, which employs functionalized nanoparticles to form protein coronas and thereby enrich circulating proteins. For protein extraction, 100 μL of serum was mixed with 400 μL of incubation buffer I and 40 μL of magnetic beads, followed by incubation at room temperature for 1 h. After magnetic separation, the supernatant was discarded, and the beads were washed twice using washing buffer. Proteins on the nanoparticles were then subjected to enzymatic digestion with a digestion buffer at 37 °C for 12–16 h. After digestion, the sample was processed through several washing and desalting steps before being concentrated, freeze-dried, and resuspended in a loading buffer for mass spectrometry analysis.

The peptides were separated using the Easy-nLC 1200 chromatography system, followed by analysis using Data-Independent Acquisition Mass Spectrometry (DIA-MS). For sample preparation, lyophilized peptides were reconstituted with 0.1% formic acid, and 500 ng of peptides were loaded for chromatographic separation. Following separation, peptides were analyzed on a QE HF-X Mass Spectrometer, the flow rate is 300 nL/min, the linear gradient is 53 min, the gradient range is 8–40% B, and the washing gradients is 7 min (liquid A: 0.1% formic acid aqueous solution; liquid B: 80% acetonitrile/0.1% formic acid). The mass spectrometry setup included a parent ion scan range of 400–1200 m/z in positive ion mode, with primary mass spectrometry (MS1) resolution set to 60,000 and secondary mass spectrometry (MS2) resolution at 15,000. The Thermo raw data was processed by Spectronaut™ software 18 (Biognosys, Schlieren, Switzerland). The analysis was conducted using the version of the human UniProt database downloaded on November 2, 2024. For the Direct-DIA search, trypsin was used as the enzyme with a specificity of P, allowing up to 3 missed cleavages. Carbamoylmethylation (+ 57.02 Da) was set as the fixed modification, while methionine oxidation (+ 15.99 Da) and acetylation (+ 42.01 Da) were set as variable modifications. The false discovery rate (FDR) for both proteins and peptides were set to 1%.

Gut microbiome analysis

The fecal samples were preserved at − 80 °C until microbial DNA extraction. DNA was extracted using the CTAB, following the manufacturer's protocol. For the blank control, nuclear-free water was used, and the total DNA was eluted in 50 μL of Elution buffer. The V3-V4 region of the bacterial 16S rRNA gene was amplified using the Universal primers 341 F (5′-CCTACGGGNGGCWGCAG-3′) and 805R (5′-GACTACHVGGGTATCTAATCC-3′). For the fungal internal transcribed spacer (ITS) region, primers ITS1FI2 (5′-GTGARTCATCGAATCTTTG-3′) and ITS2 (5′-TCCTCCGCTTATTGATATGC-3′) were applied. PCR products were assessed by 2% agarose gel electrophoresis, purified using AMPure XT beads (Beckman Coulter Genomics, Danvers, MA, USA), and quantified with Qubit (Invitrogen, USA). The amplicon pools were prepared for sequencing, with the library size and quantity determined on Agilent 2100 Bioanalyzer (Agilent, USA) and quantified using the Library Quantification Kit for Illumina (Kapa Biosciences, Woburn, MA, USA). Sequencing was carried out on an Illumina NovaSeq platform as per the manufacturer's instructions. Paired-end reads were assigned to samples using a unique barcode, followed by removal of the barcode and primer sequences. The 16S data were merged using FLASH and ITS data with Pear. Raw reads were subjected to quality filtering with fqtrim (v0.94) to obtain high-quality clean tags. Chimeric sequences were removed using Vsearch (v2.3.4). After dereplication via DADA2, feature tables and feature sequences were generated. For 16S rRNA sequencing, the number of reads per sample ranged from 63,564 to 81,180 (median 75,974). For ITS sequencing, reads per sample ranged from 40,809 to 113,622 (median 81,285). Rarefaction was performed to the depth of the sample with the fewest reads. Analyses were based on rarefied data and relative abundances without compositional bias correction. For 16S data, feature abundance was normalized to the relative abundance for each sample, and the SILVA classifier (release 138) was used for taxonomic assignment. For fungal ITS data, the relative abundance was calculated by determining the fungal count as a fraction of the total count. Alpha diversity and beta diversity were calculated using QIIME2, and sequences were normalized by random sampling to the smallest sample size. Sequence alignment for 16S was performed with BLAST and the SILVA database, while ITS sequences were classified using the RDP and Unite databases through the QIIME2 feature-classifier plugin [42].

Targeted lipidomic analysis

The 50 μL of the sample was mixed with 150 μL of water, followed by the addition of 800 μL of extract solution (MTBE: MeOH = 5:1) containing internal standards. After vortexing for 60 s, the samples were subjected to 10 min of sonication in an ice-water bath. The samples were then centrifuged at 3,000 rpm for 15 min at 4 °C, and 500 μL of the resulting supernatant was transferred into a fresh tube. The supernatant was evaporated under vacuum concentration at 37 °C. After drying, the residue was reconstituted in 150 μL of resuspension buffer (DCM: MeOH: H_2O = 60:30:4.5), vortexed for 30 s, and sonicated for 10 min in an ice-water bath. The constitution was centrifuged at 12,000 rpm for 15 min at 4 °C, and 70 μL of supernatant was carefully collected into a fresh glass vial for subsequent LC/MS analysis. A quality control (QC) sample was generated by pooling equal volumes of the supernatants from all of the samples.

UHPLC analysis was performed using a Nexera LC-40 series UHPLC System. The mobile phase A consisted of 40% water, 60% acetonitrile, 10 mmol/L ammonium acetate, and 0.1% acetic acid, while mobile phase B comprised 10% acetonitrile, 90% isopropanol, 10 mmol/L ammonium acetate, and 0.1% acetic acid. The column was maintained at a temperature of 45 °C, and the auto-sampler temperature was set to 6 °C. The injection volume was 2 μL. Mass spectrometry was conducted using a SCIEX Triple Quad™ 7500, with typical ion source parameters as follows: IonSpray Voltage: + 5500/− 4500 V, Curtain Gas: 50 psi, Temperature: 450 °C, Ion Source Gas 1:35 psi, Ion Source Gas 2:50 psi. Quantification of the target compounds was performed using SCIEX Analyst Work Station Software (Version 1.6.3) and DATA DRIVEN FLOW (Version 2.0.3.11). The absolute lipid content for each lipid class was calculated based on the peak area relative to the corresponding internal standard [43].

Statistical analysis

Statistical analyses were performed using R software (version 4.1.1, free software, see https://www.r-project.org/foundation/) and GraphPad Prism 10.3.0 (GraphPad Software Inc.). For datasets with normal distribution, multiple comparisons were performed using one-way ANOVA with Dunnett's or Tukey's post hoc analysis. The parametric Student's *t* test was used to compare two data groups with normal distribution. Fisher's exact test was employed for categorical data analysis in cases where the Chi-square test assumptions were violated, ensuring robust statistical evaluation. Data are presented as the mean values and SD unless stated otherwise. For omics data, quality control was performed. Missing values were imputed using a random sampling method based on the distribution of low-abundance signals within each experimental run. In proteomics, differential proteins between groups were identified using the *t*-test. Pathway enrichment analysis was conducted using the KEGG/GO database. For gut microbiome analysis, alpha diversity was assessed using the Chao1 and Shannon indices, reflecting species richness and diversity, respectively. Beta diversity was evaluated using Bray–Curtis distances and visualized by Principal Coordinates Analysis (PCoA). Group differences in beta diversity were analyzed using *t*-tests or ANOVA, followed by Tukey's or Dunnett's post hoc tests where appropriate. Linear Discriminant Analysis Effect Size (LEfSe) was applied to identify microbial taxa with significant differences between groups. Functional profiling of fungi was performed using FUNGuild [44], considering only highly probable and probable predictions. Taxa at higher taxonomic levels were excluded due to high functional uncertainty. Predicted trophic modes and functional groups were analyzed. For fecal lipidomics, principal component analysis (PCA) was used to visualize overall lipid distribution differences between groups. Differential lipids were identified using *t*-tests and Orthogonal Partial Least Squares Discriminant Analysis (OPLS-DA). Pathway mapping was performed using Lipid Ontology and KEGG pathways. K-means clustering was used to identify nine distinct lipid patterns, revealing abundance variation across groups. Spearman's rank correlation was used to evaluate relationships among omics datasets. Sparse Canonical Correlation Analysis (sCCA) was performed using the *mixOmics* R package to integrate gut microbiota and lipidomics profiles. Both relative abundances of microbiome and lipids were log-transformed and standardized. Optimal sparsity parameters were determined via cross-validation, and canonical variates with loading scores were obtained. Mediation analyses were performed using the *mediation* R package to examine whether PEA effects on BC were mediated by microbiome or lipids, considering both single- and combined-mediator models. Statistical significance was defined as a $p < 0.05$.

Results

PEA negatively associated with BC occurrence and invasion in human populations

The baseline characteristics of the study participants are summarized in Additional file 2: Table S2. The study cohorts comprised 3,858 individuals from the UK Biobank (1,929 diagnosed with BC) [36] and 1,135 participants from the BCPP [37], all of whom met the eligibility criteria for inclusion. Regarding the UK Biobank, after exact matching, no significant differences were observed between BC cases and non-BC controls in terms of key demographic and lifestyle factors such as age, sex, and smoking status. The mean age at baseline was 62.38 years for both BC cases and non-BC controls. Among the participants, 1,430 (74.13%) were males. The average weekly intake of dietary PEA was 0.91 g in BC cases, compared to 0.95 g in non-BC controls ($p < 0.001$).

Regarding the BCPP cohort, 1,135 BC patients were included, with disease stages as follows: 596 (52.51%) at the Ta stage, 302 (26.61%) at the T1 stage, and 237 (20.88%) at the ≥ T2 stage. Participants diagnosed with the lowest BC stage (Ta) had a mean age of 68.85 years, while those in the most advanced BC stage (≥ T2) had a mean age of 72.67 years ($p = 0.206$). The median weekly dietary PEA was higher among individuals with the lowest BC stage (Ta) at 1.84 g, whereas those with the most advanced stage (≥ T2) had a lower weekly dietary PEA at the median of 1.68 g ($p = 0.036$).

The association between dietary PEA and BC occurrence was examined using data from the UK Biobank (Table 1). After exact matching, per SD increase in dietary PEA associated with a lower risk of BC (OR = 0.93, 95% CI: 0.87–0.99, $p = 0.028$) adjusted for BMI, qualification, household income, and ethnicity.

We further assessed the associations of PEA with BC invasion in the BCPP. Specifically, per SD increase in dietary PEA associated with 13% lower risk of being diagnosed with higher BC stage (OR = 0.87, 95% CI 0.77–0.97, $p = 0.015$) in the adjusted model. In sensitivity analysis comparing NMIBC vs. MIBC, per SD increase in dietary PEA associated with a 17% lower risk of development of muscle-invasive disease (OR = 0.83, 95% CI 0.71–0.97, $p = 0.022$) with adjustments for sex, age, smoking status, and ethnicity. These findings were consistent across both the UK Biobank and the BCPP cohorts, suggesting that dietary PEA overall negatively associated with both the occurrence and invasion of BC by population-based data.

PEA inhibits the migration, invasion, and proliferation of EJ and T24 BC cells

To further explore the effects of PEA on BC, we performed a series of in vitro experiments using EJ and T24 BC cells with and without PEA treatment. We utilized wound healing assays and transwell assays to assess the impact of PEA on the migration and invasion abilities of EJ and T24 BC cells. Additionally, CCK-8 assays were conducted to evaluate the effect of PEA on BC cell proliferation.

The wound healing assay results revealed that PEA significantly inhibited the migration ability of EJ BC cells (Fig. 1H & I). In the transwell assay, PEA treatment markedly suppressed the invasion ability of EJ BC cells compared to control group ($p < 0.0001$) (Fig. 1J & K). In the CCK-8 assay with or without PEA treatment, we measured cell proliferation at 24, 48, and 72 h. At all-time points, the cell viability for PEA-treated group was consistently lower than that for control group, which was set

Table 1 Associations between dietary PEA and the risk of BC occurrence and invasion in participants from the UK Biobank and the BCPP[a]

	Method	BC occurrence risk/BC invasion risk	BC Case/N	Dietary PEA	
				OR (95% CI)	*p* value
Dietary PEA-BC occurrence					
UK Biobank	Binomial Logistic Regression	model 1[b]	1,929/3,858	0.93 (0.86, 0.98)	0.022
		model 2		0.92 (0.86, 0.99)	0.016
		model 3		0.93 (0.87, 0.99)	0.028
Dietary PEA-BC invasion					
BCPP	Ordinal Logistic Regression	model 1[c]	1,135	0.87 (0.78, 0.97)	0.013
		model 2		0.87 (0.78, 0.97)	0.015
		model 3		0.87 (0.77, 0.97)	0.015
BCPP NMIBC vs. MIBC	Binomial Logistic Regression	model 1	1,135	0.86 (0.73, 0.98)	0.026
		model 2		0.84 (0.72, 0.97)	0.022
		model 3		0.83 (0.71, 0.97)	0.022

[a] The association of dietary PEA with the occurrence of BC is examined using the data of the UK Biobank, while the relationship of dietary PEA and BC invasion was analyzed using data from the BCPP

[b] Regarding the analysis of the UK Biobank, after exact matching, no significant differences were found between BC cases and non-BC controls in age, sex, or smoking status. Thus, model 1 was performed without covariate adjustments; model 2: adjusted for BMI (kg/m^2; continuous); model 3: additionally adjusted for qualification (categorical), household income (categorical), and ethnicity [defined as a categorical variable as follows: 0 (white); 1 (non-white); 2 (prefer not to answer)]

[c] model 1: crude model without adjustment; model 2: adjusted for age (years, continuous) and smoking status [defined as a categorical variable as follows: 0 (never smokers); 1 (ever smokers); 2 (current smokers)]; model 3: additionally adjusted for ethnicity [defined as a categorical variable as follows: 0 (white); 1 (non-white)]

PEA Pentadecanoic acid, *BC* bladder cancer, *BCPP* The Bladder Cancer Prognosis Programme, *OR* odds ratio, *CI* confidence interval;confidence interval, *NMIBC* non-muscle-invasive bladder cancer, *MIBC* muscle-invasive bladder cancer at 100%, indicating a significant reduction in cell proliferation ($p = 0.0036$) (Fig. 1L). Similar results were observed in T24 BC cells (Additional file 2: Figure S1). These in vitro findings demonstrate that PEA effectively inhibits EJ and T24 BC cells' migration, invasion, and proliferation, highlighting its potential benefits in BC.

PEA protects against the occurrence and invasion of BC in a N-butyl-N-(4-hydroxybutyl) nitrosamine (BBN)-induced mouse model

We assessed the effect of PEA on BC in a BBN-induced mouse model, where mice were treated with daily gavage of two different doses of PEA. Mice were euthanized at designated time points to comprehensively evaluate the occurrence and invasion of BC. As described in the " Methods" section, mice were divided into 4 groups: control group, BC model group, low-dose PEA-treated with BBN-induced group (BC PEAL), and high-dose PEA-treated with BBN-induced group (BC PEAH) at each stage. Throughout both the occurrence and invasion stages, PEA-treated mice demonstrated significantly lower weight gain compared to BC model group and control group ($p < 0.05$) (Fig. 1B).

BC development was assessed based on the presence or absence of tumors, histopathological analysis (including normal tissue, reactive atypia, dysplasia, carcinoma in situ (CIS), early invasion, and invasion), as well as the Ki-67-positive cell index in bladder tissue sections. To examine the impact of PEA on BC occurrence, mice were euthanized at week 15 (Fig. 1A). Histopathological examination and Ki-67 quantification revealed a marked increase in BC occurrence in BC model and PEA-treated groups compared to control group. Specifically, histological analysis showed that mice in BC PEAH group exhibited significantly fewer pathological changes compared to BC model group ($p = 0.015$). Additionally, Ki-67 positive cells in bladder tissue were significantly reduced in both BC PEAH ($p = 0.008$) and BC PEAL ($p = 0.035$) groups compared to BC model group, suggesting a potential inhibitory effect of PEA on the occurrence of BC model (Fig. 1C–G).

For the invasion stage, mice were euthanized at week 23 (Fig. 1A). While a trend suggesting a protective effect of PEA on BC invasion was observed, the results did not reach statistical significance (Fig. 1C–G).

Collectively, these findings indicate that PEA has a potential inhibitory effect on both the occurrence and invasion of BC in the BBN-induced mouse model, particularly in the early stages of cancer development.

PEA modulates lipid metabolism-related pathways in BC mice through proteomic analysis

To investigate the impact of PEA on protein profiles, we conducted a comprehensive proteomic analysis of serum samples from mice using DIA-MS. A total of 1,368 proteins were detected across all groups, with missing values imputed using random sampling from a distribution of low-abundance signals within each run.

We performed differential analysis on serum proteins between PEA-treated groups (i.e., BC PEAL and BC PEAH) and BC model group at both the occurrence and invasion stages. At the occurrence stage, 33 proteins (8 upregulated and 25 downregulated) were differentially expressed ($p < 0.05$) in BC PEAL group compared to BC model group, and 25 proteins (11 upregulated and 14 downregulated) were differentially expressed ($p < 0.05$) in BC PEAH group compared to BC model group (Fig. 2A; Additional file 4: Table S3). Pooled data from both comparisons identified 53 unique proteins, with five proteins—Efcab3, Prss59, Pcbp1, Try10, and Prss3b—showing overlapped in both comparison groups (Fig. 2B). Efcab3 and Prss59 are proposed to be involved in calcium signaling and proteolytic processes respectively, while Try10, a serine protease, may contribute to tumor-related protease activity, highlighting their potential roles in cancer [45]. Notably, Pcbp1, an RNA-binding protein, has been shown to play a dual role in cancer immunity: it supports effector T-cell functions that help suppress tumor growth, but when dysregulated, it may contribute

(See figure on next page.)

Fig. 1 PEA inhibits BC tumorigenesis in vitro and in vivo model. **A** Flowchart of animal experiment design ($n = 10$/group). **B** Body weight gain in groups (BC model, BC PEAL, BC PEAH, and control) over time. **C–G** PEA protects against BC occurrence and invasion in a BBN-induced mouse model, including **C** representative pictures of bladder tissue and **D** representative images of H&E-stained bladder tissue. Scale bar is 100 µm. **E** Percentage of mice in each group showing normal tissue, reactive atypia, dysplasia, CIS, early invasion, and invasion at BC occurrence stage (left) and BC invasion stage (right). **F** Representative images of Ki-67 staining. Scale bar is 100 µm. **G** Percentage of Ki-67 positive cells in groups at BC occurrence stage (left) and BC invasion stage (right). **H–L** PEA inhibits the migration, invasion, and proliferation of EJ BC cells, including **H** images of the wound healing assay indicating migration abilities of EJ BC cells treated with or without PEA at different time points. **I** Migration closure of cells treated with or without PEA. **J** Images of transwell assay of EJ BC cells treated with or without PEA. **K** Invasion cells numbers of EJ BC cells treated with or without PEA. **L** CCK-8 assay showing the proliferation of EJ BC cells treated with or without PEA at 24, 48, and 72 h. Statistical significance is indicated by asterisks (*$p < 0.05$, **$p < 0.01$, ***$p < 0.001$, ****$p < 0.0001$). Abbreviations: PEA, pentadecanoic acid; BC, bladder cancer; BC PEAL, low-dose PEA-treated group; BC PEAH, high-dose PEA-treated group

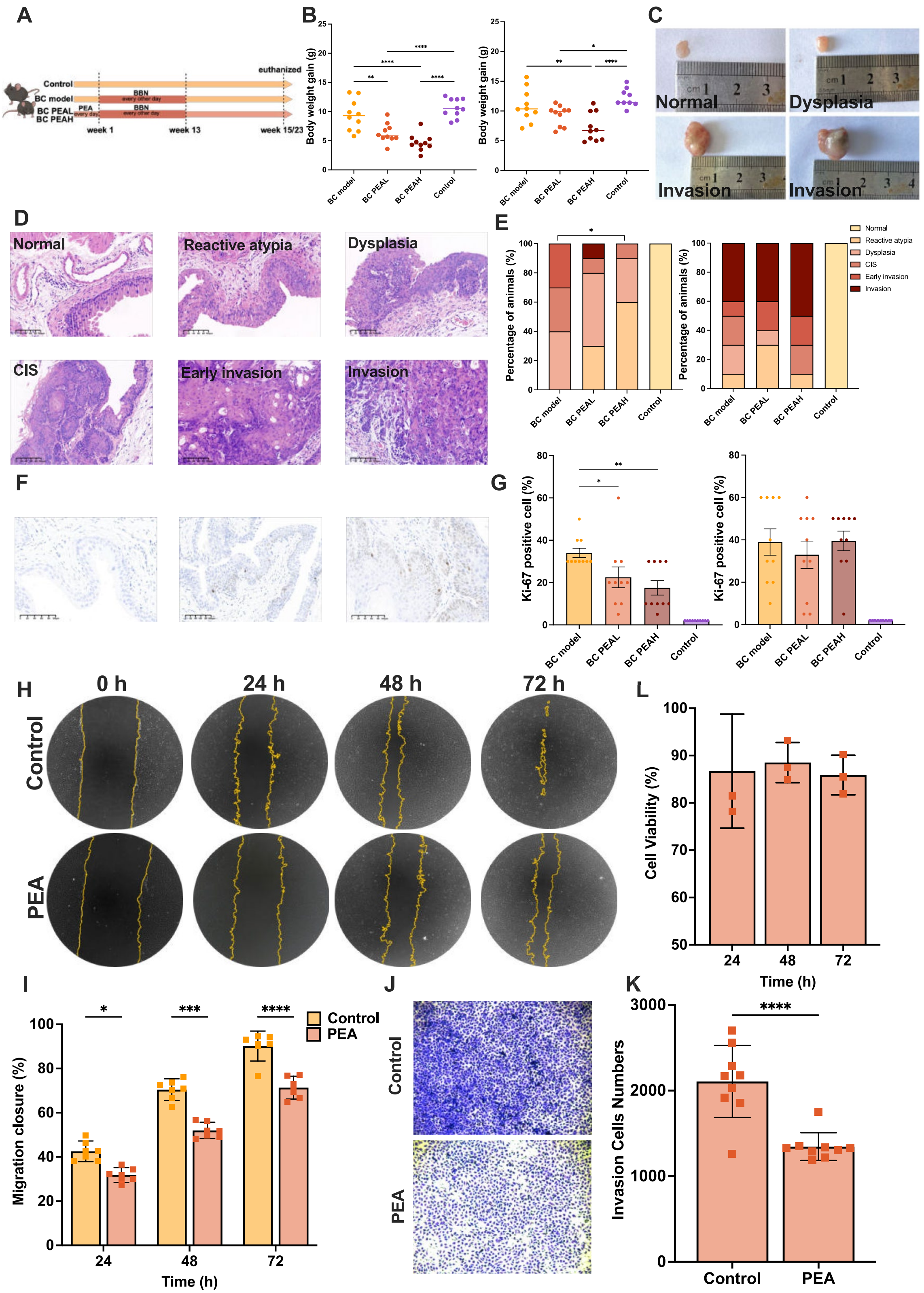

Fig. 1 (See legend on previous page.)

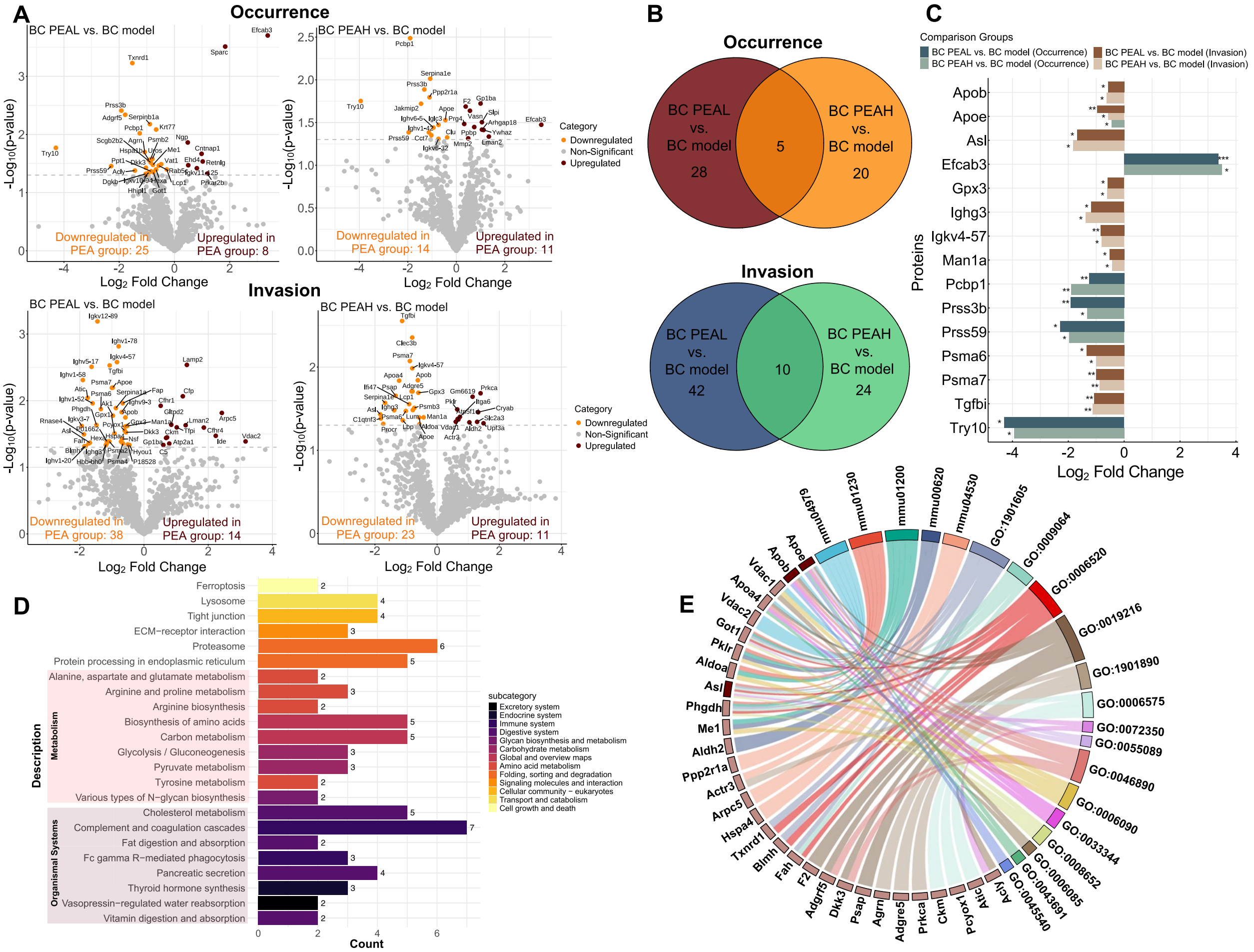

Fig. 2 PEA modulates lipid metabolism-related pathways in BC mice through proteomic analysis. **A** Differential analysis comparing PEA-treated groups (i.e., BC PEAL and BC PEAH) with the BC model at BC occurrence and invasion stages. Orange represents downregulated proteins, while dark red indicates upregulated proteins. **B** Venn diagram showing differentially expressed proteins across comparison groups at BC occurrence and invasion stages. **C** Log_2FC and *p*-values of 15 PEA-DEPs across different comparison groups (BC PEAL and BC PEAH vs. BC model) at BC occurrence and invasion stages. Light green and green indicate comparison groups at the BC occurrence stage, while khaki and brown indicate comparison groups at the BC invasion stage. Statistical significance is indicated by asterisks (*$p < 0.05$, **$p < 0.01$, ***$p < 0.001$). **D** KEGG pathway enrichment analysis of the identified proteins, with the *x*-axis showing the protein gene count enriched in each pathway. **E** The chord plot showed 20 significant KEGG and GO pathways related to metabolism and organismal systems, with proteins enriched in these pathways. Deep red highlights the PEA-DEPs. Pathways include mmu04979: Cholesterol metabolism; mmu01230: Biosynthesis of amino acids mmu01200: Carbon metabolism; mmu00620: Pyruvate metabolism; mmu04530: Tight junction; GO:1901605: Alpha-amino acid metabolic process; GO:0009064: Glutamine family amino acid metabolic process; GO:0006520: Amino acid metabolic process; GO:0019216: Regulation of lipid metabolic process; GO:1901890: Positive regulation of cell junction assembly; GO:0006575: Cellular modified amino acid metabolic process; GO:0072350: Tricarboxylic acid metabolic process; GO:0055089: Fatty acid homeostasis; GO:0046890: Regulation of lipid biosynthetic process; GO:0006090: Pyruvate metabolic process; GO:0033344: Cholesterol efflux; GO:0008652: Amino acid biosynthetic process; GO:0006085: Acetyl-CoA biosynthetic process; GO:0043691: Reverse cholesterol transport; GO:0045540: Regulation of cholesterol biosynthetic process. Abbreviations: PEA, pentadecanoic acid; BC, bladder cancer; FC, fold change; PEA-DEP, PEA-differentially expressed protein; BC PEAL, low-dose PEA-treated group; BC PEAH, high-dose PEA-treated group

to the creation of an immunosuppressive environment that facilitates tumor progression [46]. Furthermore, the human ortholog of Prss3b has been associated with cancer progression and metastasis, with its expression levels correlating with tumor aggressiveness and poor prognosis [47–49].

At the invasion stage, the differential analysis identified 52 proteins (14 upregulated and 38 downregulated) in BC PEAL group, while 34 proteins (11 upregulated and 23 downregulated) in BC PEAH group, both compared to BC model group ($p < 0.05$) (Fig. 2A; Additional file 4: Table S3). Pooled results revealed 76 unique proteins, with 10 overlapped proteins between the two groups: i.e., Apoe, Ighg3, Igkv4-57, Man1a, Apob, Gpx3, Tgfbi, Asl, Psma6, and Psma7. Among these, Apoe and Apob, key apolipoproteins involved in lipid metabolism, are enriched in cholesterol metabolism pathways and are also implicated in cancer through their effects on the tumor microenvironment [50]. Moreover, Ighg3 regulates tumor cell proliferation, invasion, metastasis, and immune microenvironment, while Gpx3 influences tumor cell proliferation, migration, and invasion by scavenging reactive oxygen species, both of which are closely linked to cancer progression [51, 52].

The 5 overlapped proteins from the occurrence stage and the 10 overlapped proteins from the invasion stage were categorized as PEA-differentially expressed protein (PEA-DEP). Among these 15 PEA-DEPs, only Efcab3 was upregulated in PEA-treated groups, while the remaining 14 proteins were downregulated compared to BC model group (Fig. 2C).

When pooling the differentially expressed proteins (DEPs) from all comparison groups (BC PEAL vs. BC model and BC PEAH vs. BC model) at both the occurrence and invasion stages, a total of 122 unique proteins were identified ($p<0.05$). We then performed KEGG and GO pathway enrichment analyses on these proteins (Fig. 2D; Additional file 2: Figure S2). The results revealed several enriched pathways related to metabolism and organismal systems, including pathways potentially linked to gut microbiome, such as cholesterol metabolism, amino acid biosynthesis, carbon metabolism, pyruvate metabolism, and tight junctions (Fig. 2D). Gut microbiome influences cholesterol metabolism by converting cholesterol to coprostanol, incorporating it into bacterial membranes, and metabolizing bile acids, which in turn affect host cholesterol absorption, synthesis, and excretion [53]. By fermenting dietary fibers and carbohydrates, gut microbiome produces metabolites like fatty acids and tryptophan metabolites, which modulate host carbon and pyruvate metabolism, as well as amino acid biosynthesis, all of which are critical in regulating host physiology and disease progression [15, 54, 55]. Tight junctions in the intestinal epithelium are regulated by gut microbiome, which modulates the expression of tight junction proteins, helping to maintain intestinal barrier integrity and influencing gut health.

Among the proteins enriched in these pathways, three of the 15 PEA-DEPs—i.e., Apoe, Apob, and Asl—were identified as potentially linked to gut microbiome-related pathways (Fig. 2E). Both Apoe and Apob, essential regulators of lipid metabolism, interact with the gut microbiome to modulate lipid metabolism [56]. Asl, which plays a key role in arginine metabolism by converting argininosuccinate to arginine and fumarate, influences energy metabolism and potentially regulates lipid metabolism. As the biologically active form of arginine, L-arginine is also crucial in host-microbe interactions and has been linked to regulating lipid metabolism [57].

Overall, the differential proteins induced by PEA and their enriched pathways suggest that gut microbiome may play a regulatory role in modulating these pathways, thereby affecting the occurrence and invasion of BC.

PEA induces distinct and beneficial modulation of gut bacteria and fungi

To identify specific microbiota that may be dysregulated in PEA-treated groups with potential protective effects against BC occurrence and invasion, we sequenced the 16S rRNA for bacterial communities and the ITS for fungal communities from fecal samples collected at both the occurrence and invasion stages across all groups.

PEA enhances gut bacterial diversity and modulates key taxa in BC

At the phylum level, p_*Firmicutes* and p_*Bacteroidota* were identified as the dominant bacterial phyla across groups. p_*Verrucomicrobiota* was notably more abundant in PEA-treated and control groups than in BC model group, while p_*Desulfobacterota* was more abundant in BC model group than in PEA-treated and control groups. The genus-level abundance analysis also reflected these trends, with g_*Akkermansia* (belonging to p_*Verrucomicrobiota*) and g_*Desulfovibrio* (belonging to p_*Desulfobacterota*) exhibiting the same patterns, suggesting that PEA may promote the growth of p_*Verrucomicrobiota* while inhibiting p_*Desulfobacterota* (Additional file 2: Figure S3 & S4).

At the occurrence stage, the PCoA plot did not show a clear separation between groups, with considerable overlap. However, variations in microbial composition were detectable across groups using the Bray–Curtis metric, which assesses the dissimilarity between microbial communities (Fig. 3A & B). In contrast, at the invasion stage, both alpha diversity indices (i.e., Chao1 and Shannon) and the beta diversity metrics (i.e., Bray–Curtis) revealed significant differences between PEA-treated groups and BC model group (Fig. 3A & C). These results suggest that PEA intervention increases the gut microbial diversity in BC mice.

To further investigate the specific bacterial changes associated with PEA, we compared the microbiome profiles between BC PEAL group and BC model group, and between BC PEAH group and BC model group, at both the occurrence and invasion stages using LEfSe. At the occurrence stage, 206 bacterial taxa were differentially expressed between BC PEAL group and BC model group. In comparison, 82 taxa showed significant differences between BC PEAH and BC model groups. Among these, 22 bacterial taxa overlapped between the two comparisons ($p < 0.05$, LDA > 2). At the invasion stage, 97 bacterial taxa were differentially expressed between BC PEAL group and BC model group, and 200 taxa were differentially expressed between BC PEAH group and BC model group. Of these, 51 bacterial taxa overlapped between the two comparisons ($p < 0.05$, LDA > 2) (Fig. 3D & E; Additional file 4: Table S4).

In total, 62 unique bacterial taxa were identified from both stages, with 11 taxa shared between the occurrence and invasion stages. These overlapped taxa were categorized as PEA-differentially enriched bacterium (PEA-DEB) (Fig. 3F).

PEA influences gut fungal taxa, specifically in BC invasion

In fungi, the taxonomic composition at both the occurrence and invasion stages revealed similar patterns. At the phylum level, p_*Ascomycota* was the dominant group. At the genus level, g_*Kazachstania* (belonging to p_*Ascomycota*) predominated across all groups (Additional file 2: Figure S5). Consistently, neither alpha diversity indices (i.e., Chao1 and Shannon) nor beta diversity (i.e., Bray–Curtis) revealed significant differences across groups at both the occurrence and invasion stages (Fig. 4A–C).

To further investigate the fungal changes associated with PEA, we compared BC PEAL and BC model groups, as well as BC PEAH and BC model groups, at both the occurrence and invasion stages using LEfSe. At the occurrence stage, 15 fungal taxa were differentially expressed between BC PEAL group and BC model group, while only four taxa showed significant differences between BC PEAH group and BC model group. Notably, no overlapped taxa were found between the two comparisons ($p < 0.05$, LDA > 1.5). At the invasion stage, 17 fungal taxa were differentially expressed between BC PEAL group and BC model group, while 18 taxa exhibited differential expression between BC PEAH group and BC model groups ($p < 0.05$, LDA > 1.5) (Fig. 4D & E; Additional file 4: Table S5). Among these, 7 fungal taxa overlapped between the two comparisons, which were categorized as PEA-differentially enriched fungus (PEA-DEF) (Fig. 4F).

To explore the potential functional implications of the observed PEA-induced fungal changes, FUNGuild analysis was performed by pooling the differentially expressed fungus (DEF) from all comparison groups at both occurrence and invasion stages. The results revealed that PEA intervention increased the proportion of saprotrophic fungi and decreased potential pathogens compared to the model group (Additional file 4: Table S6 & Additional file 2: Figure S6).

PEA modulates lipid metabolism through gut microbiome at BC occurrence and invasion

We explored potential connections between the bacteria (11 PEA-DEBs), fungi (7 PEA-DEFs), and proteins (15 PEA-DEPs) changes induced by PEA based on Spearman correlation (Fig. 5A; Additional file 4: Table S7 & S8). The two apolipoproteins, which are enriched in the cholesterol metabolism pathway—i.e., Apoe and Apob—showed significant correlations with the gut microbiome. Apob was positively correlated with all 7 PEA-DEFs ($p < 0.05$), while Apoe exhibited significant negative correlations with three specific PEA-DEBs: g_*Alistipes*, s_*Alistipes*_unclassified, and s_*uncultured*_Alistipes_sp ($p < 0.05$). These findings suggest a potential modulation of lipid metabolism through gut microbiome by PEA, which could contribute to its protective effects against BC.

To elucidate the role of lipid metabolism in the effect of PEA on BC, we performed a fecal-targeted lipidomic analysis, identifying a total of 950 lipids classified into five major classes and 23 subclasses. Triacylglycerols (TAG) dominated the composition (31.37%, comprising 298 lipids), followed by phosphatidylethanolamines (PE) with 103 lipids (10.84%) and phosphatidylglycerol (PG) with 88 lipids (9.26%) (Additional file 2: Figure S7). PCA revealed that lipidomic profiles among groups were not distinctly separated, necessitating further statistical analysis to identify key discriminatory lipids (Additional file 2: Figure S8). Differential lipid analysis, based on both Student's *t* test ($p < 0.05$) and OPLS-DA with Variable Importance in Projection (VIP) ≥ 1, identified 78 significant lipids in BC PEAH group compared to BC model group at the stage of occurrence and invasion, including

(See figure on next page.)

Fig. 3 PEA enhances gut bacterial diversity and modulates key taxa in BC. **A** Alpha-diversity analysis using the Chao1 and Shannon index at BC occurrence and invasion stage. **B, C** Beta-diversity analysis, including PCoA and Bray–Curtis distance, with PERMANOVA testing for differences between groups at BC occurrence and invasion stage. **D** LEfSe analysis identifying differentially abundant taxa between PEA-treated (i.e., BC PEAL and BC PEAH) and BC model at BC occurrence and invasion stages, presenting the top 30 taxa with $p < 0.05$ and LDA > 3. **E** Venn diagram showing the differential bacterial taxa across comparison groups at BC occurrence and invasion stages ($p < 0.05$, LDA > 2). **F** Identification of marker bacterial taxa differentiating PEA-treated groups and BC model ($p < 0.05$, LDA > 2), with taxa in red indicating PEA-DEBs. Statistical significance is indicated by asterisks (*$p < 0.05$, **$p < 0.01$, ***$p < 0.001$). Abbreviations: PEA, pentadecanoic acid; BC, bladder cancer; PCoA, principal coordinates analysis; LEfSe, linear discriminant analysis effect size; LDA, linear discriminant analysis; PEA-DEB, PEA-differentially enriched bacterium

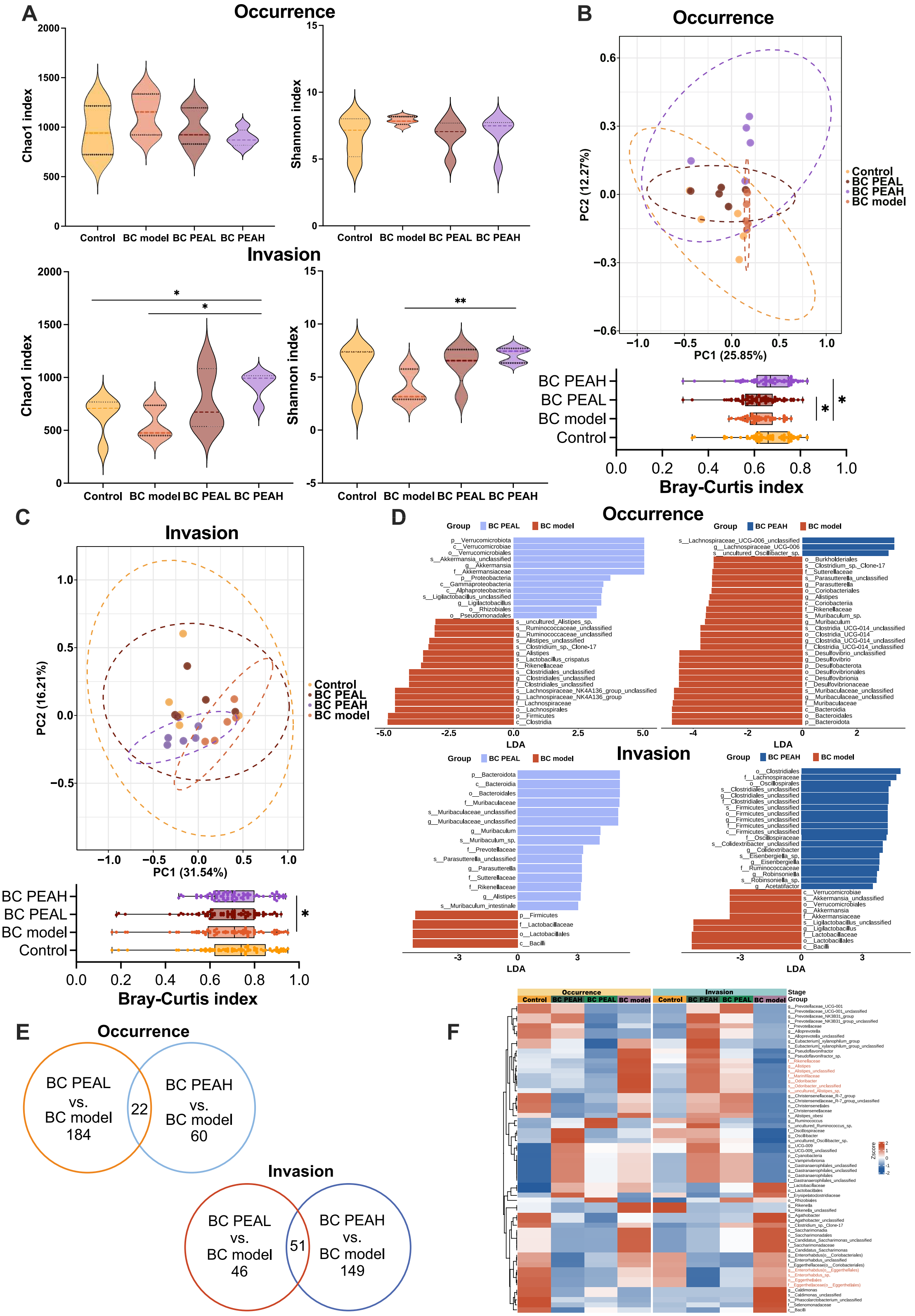

Fig. 3 (See legend on previous page.)

59 upregulated and 19 downregulated lipids. In comparison, 47 significant lipids were found in BC PEAL group compared to BC model group at the stage of occurrence and invasion, with 38 upregulated and 9 downregulated lipids (Fig. 6A; Additional file 4: Table S9). Among them, 11 lipids overlapped between the above comparison groups and were categorized as PEA-differentially expressed lipids (PEA-DELs) (Fig. 6B). Pathway mapping analysis of the PEA-DELs identified pathways including lipid metabolism (i.e., glycerophospholipid metabolism, arachidonic acid metabolism, linoleic acid metabolism), membrane structure and signaling (i.e., glycosylphosphatidylinositol (GPI)-anchor biosynthesis, endocannabinoid signaling), autophagy, one-carbon metabolism, and cancer-related metabolic pathways involving choline and folate metabolism (Additional file 4: Table S10). Collectively, these pathways may underlie potential mechanisms linking PEA-DELs to BC. *Z*-score normalization further demonstrated that most of these 11 PEA-DELs were upregulated in PEA-treated groups compared with the BC model group, except for TG(58:7)_FA(22:5), a triacylglycerol with a total of 58 carbon atoms and 7 double bonds, with one fatty acid chain consisting of 22 carbon atoms and 5 double bonds, and HexCer(18:0/24:1), a hexosylceramide with an 18-carbon saturated fatty acid and a 24-carbon monounsaturated fatty acid, which were downregulated (Fig. 6C).

To explore the potential interactions between lipid metabolism and the gut microbiome, we performed Spearman correlation analysis of these 11 PEA-DELs with 11 PEA-DEBs and 7 PEA-DEFs. Most lipids showed a significant negative correlation with o_*Eggerthellales*, f_*Eggerthellaceae*, g_*Enterorhabdus*, and s_*Enterorhabdus*_sp, while HexCer(18:0/24:1) exhibited a significant positive correlation with these bacteria; additionally, PE(18:0_20:1), a phosphatidylethanolamine consisting of an 18-carbon saturated fatty acid and a 20-carbon monounsaturated fatty acid, was negatively correlated with c_*Leotiomycetes* ($p < 0.05$) (Fig. 6D; Additional file 4: Table S11). However, the identified lipid metabolism-associated gut microbiota, including g_*Alistipes*, s_*Alistipes*_unclassified, s_uncultured_*Alistipes*_sp, and all PEA-DEFs did not show significant correlations with any of these PEA-DELs.

Further investigation using *K*-means clustering to examine the relative abundance patterns of all DELs across groups identified 9 distinct clusters, each exhibiting unique trends. Notably, Clusters 5, 7, and 8 showed consistent directional changes in BC model groups of both the occurrence and invasion stages compared to PEA-treated groups, indicating their potential involvement in BC (Fig. 6E; Additional file 4: Table S12). Further correlation analysis of these clusters with PEA-DEBs and PEA-DEFs revealed that Cluster 8 significantly negatively correlated with g_*Alistipes*, including s_*Alistipes*_unclassified, and s_uncultured_*Alistipes*_sp (Fig. 6F; Additional file 4: Table S13). Importantly, Cluster 8 contained two of the PEA-DELs, PE(18:0_20:1) and PE(O-18:0_20:1), both of which are phosphatidylethanolamines consisting of an 18-carbon saturated fatty acid and a 20-carbon monounsaturated fatty acid, with or without an alkyl ether substituent (Fig. 6G). Sparse Canonical Correlation Analysis (sCCA) and mediation analyses were performed to further investigate the co-varying patterns among PEA-DEBs, PEA-DEFs, and PEA-DELs as well as their potential mediating role in the relationship between PEA and BC. Accordingly, sCCA identified two significant canonical variates ($r = 0.918$ and $r = 0.735$), both showing high loadings for *Alistipes* taxa (g_*Alistipes*, s_*Alistipes*_unclassified, and s_uncultured_*Alistipes*_sp), and phosphatidylethanolamines [PE(18:0_20:1) and PE(O-18:0_20:1)] (Additional file 2: Figure S9). In mediation analyses, direct effects of PEA were generally negative and in combined-mediator models including s_uncultured_*Alistipes*_sp. and PE(18:0_20:1), as well as in models additionally including PE(O-18:0_20:1), both direct and indirect effects were negative but non-significant (Additional file 4: Table S14). Additionally, an association analysis of 11 DELs and 15 DEPs, which confirmed that Apoe and Asl were indeed associated with PE(18:0_20:1) and PE(O-18:0_20:1) ($p < 0.05$), confirming the results (Additional file 2: Figure S10; Additional file 4: Table S15). Collectively, these findings suggest that *Alistipes* taxa may influence lipid metabolism, particularly

(See figure on next page.)

Fig. 4 PEA influences gut fungal taxa, specifically in BC invasion. **A** Alpha-diversity analysis using the Chao1 and Shannon index at BC occurrence and invasion stage. **B, C** Beta-diversity analysis, including PCoA and Bray–Curtis distance, with PERMANOVA testing for differences between groups at BC occurrence and invasion stage. **D** LEfSe analysis identifying differentially abundant taxa between PEA-treated groups (i.e., BC PEAL and BC PEAH) and BC model at BC occurrence and invasion stages ($p < 0.05$, LDA > 1.5). **E** Venn diagram showing the differential fungal taxa across comparison groups at BC occurrence and invasion stages ($p < 0.05$, LDA > 1.5). **F** Identification of marker fungal taxa differentiating PEA-treated groups and BC model ($p < 0.05$, LDA > 1.5), with taxa in red indicating PEA-DEFs. Statistical significance is indicated by asterisks (*$p < 0.05$, **$p < 0.01$, ***$p < 0.001$). Abbreviations: PEA, pentadecanoic acid; BC, bladder cancer; PCoA, principal coordinates analysis; LEfSe, linear discriminant analysis effect size; LDA, linear discriminant analysis; PEA-DEF, PEA-differentially enriched fungus

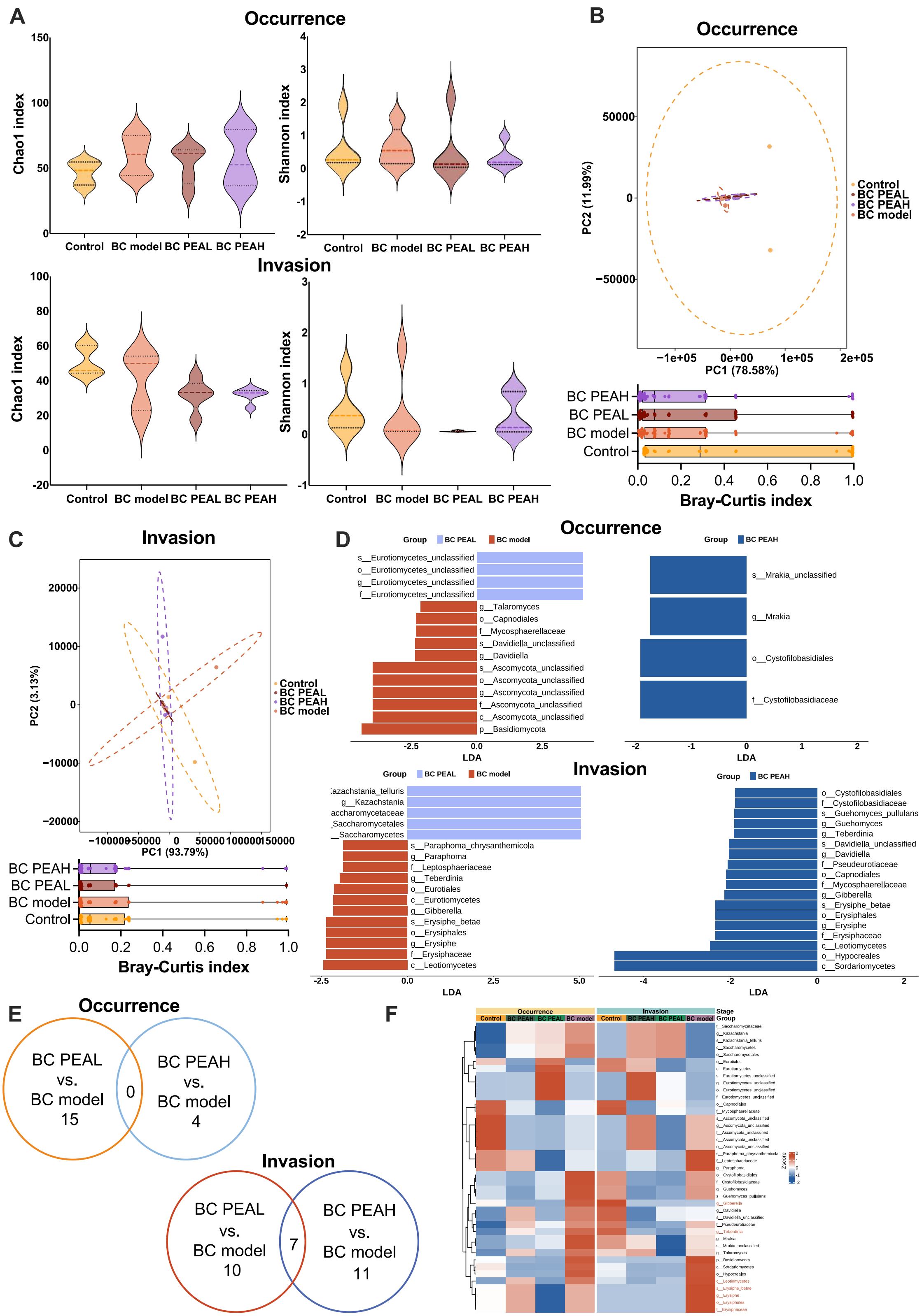

Fig. 4 (See legend on previous page.)

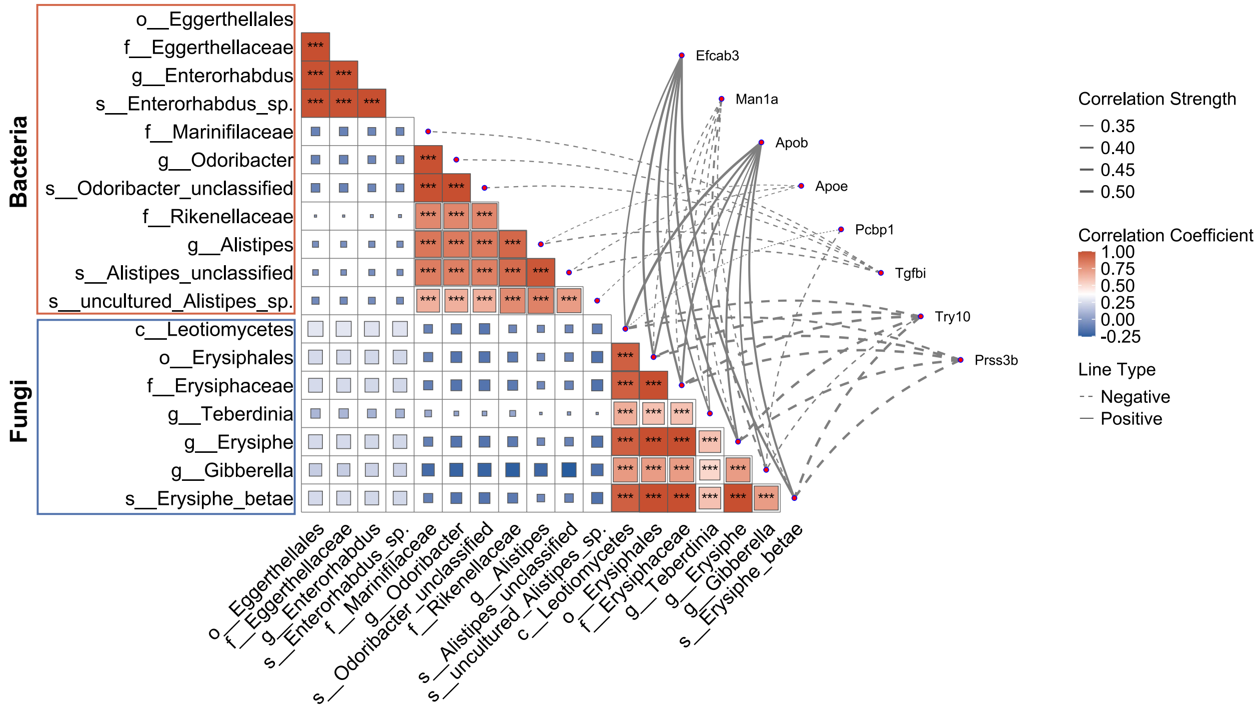

Fig. 5 Spearman correlation analysis exploring potential interactions between PEA-induced changes in bacterial, fungal, and protein profiles. The heatmap depicts correlations among 11 PEA-DEBs (red boxes) and 7 PEA-DEFs (blue boxes). Correlation strength is indicated by the color of the squares in the heatmap, with red representing higher correlations and blue representing lower ones. Statistical significance is indicated by asterisks (*$p<0.05$, **$p<0.01$, ***$p<0.001$), with the size of the squares reflecting the *p*-values (smaller *p*-values are represented by larger squares). The connecting line represents correlations between both PEA-DEBs and PEA-DEFs and 15 PEA-DEPs. The thickness of the lines indicates the correlation strength, with solid lines representing positive correlations and dashed lines representing negative correlations. Abbreviations: PEA, pentadecanoic acid; PEA-DEP, PEA-differentially expressed protein; PEA-DEB, PEA-differentially enriched bacterium; PEA-DEF, PEA-differentially enriched fungus

through regulating lipid PE in Cluster 8, which could impact membrane remodeling, autophagy, one-carbon metabolism, and cancer-related metabolic pathways such as choline and folate metabolism, thereby playing a role in BC.

Discussion

Growing evidence suggests that OCFAs, such as PEA, which is abundant in dairy products and ruminant meat, confer various health benefits, potentially mediated in part by their prebiotic effects on the gut microbiome [1, 19]. However, the impact of PEA on gut microbiome composition and function in humans remains poorly understood. To elucidate the underlying mechanisms linking the gut and bladder, we conducted an integrative study combining population-based analysis with in vitro and in vivo experiments. Our findings provide evidence that PEA exerts its protective effects against BC via the *gut-bladder* axis, primarily through the modulation of lipid metabolism, which is consistent with the perspective put forward by Shuai et al. [58], highlighting the close interplay between the gut microbiome and host metabolism. This offers new insights into BC prevention and intervention strategies.

Although associations between PEA and BC have been scarcely reported, our study is the first to demonstrate that higher intake of dietary PEA is significantly associated with lower risk of BC occurrence and invasion. This observation is further supported by our in vitro experiments, which revealed that PEA exhibits anti-cancer effects in EJ and T24 BC cells. Specifically, PEA inhibited cell migration and invasion, suggesting its potential to disrupt signaling pathways involved in cancer cell motility and metastasis. Moreover, its suppression of cell proliferation indicates a possible role in interfering with cell cycle progression or inducing apoptosis. These findings align with those of To et al. [24], who reported that PEA can inhibit the migratory and invasive capabilities of cancer stem-like cells by targeting the JAK2/STAT3 signaling pathway.

Consistent with our population-based and in vitro findings, we validated the protective effects of PEA in a BBN-induced BC mouse model, where PEA administration significantly reduced both BC occurrence and invasion.

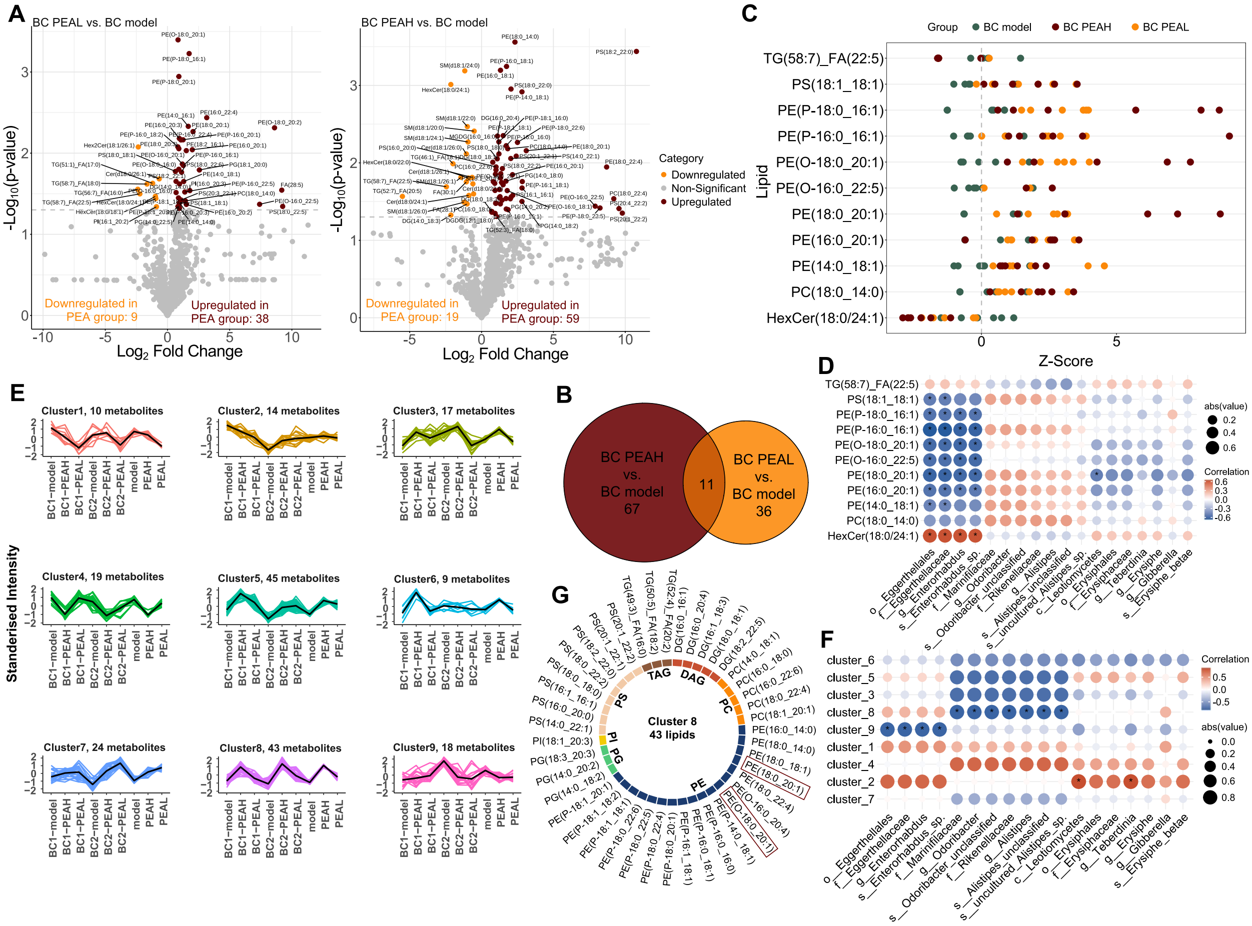

Fig. 6 PEA modulates lipid metabolism through gut microbiome at BC occurrence and invasion. **A** Differential analysis comparing PEA-treated groups (i.e., BC PEAL and BC PEAH) with BC model. Orange represents downregulated lipids, while dark red indicates upregulated lipids ($p < 0.05$, VIP ≥ 1). BC PEAL groups, BC PEAL groups, and BC model groups in differential analysis of lipids include the groups at BC occurrence and invasion. **B** Venn diagram showing differentially expressed lipids across comparison groups (i.e., BC PEAL vs. BC model and BC PEAH vs. BC model). **C** The *Z*-score plot of the 11 PEA-DELs. The *Z*-scores were calculated to normalize the differential lipids across different samples. The *x*-axis represents the *Z*-score values, and the *y*-axis represents the differential lipids. Points in different colors represent samples from different groups (i.e., BC PEAL, BC PEAH, and BC model). **D** Spearman correlation analysis between 11 PEA-DELs and both PEA-DEBs and PEA-DEFs. Correlation strength and direction are indicated by the color of the circles in the heatmap, with blue representing negative correlations and red representing positive correlations. The size of the circles reflects the absolute value of the correlation coefficient, with larger circles indicating stronger correlations. Asterisks indicate statistical significance (*$p < 0.05$). **E** *K*-means clustering analysis of differential lipids across all comparison groups. The *x*-axis represents the sample group names (BC1 represents the samples at the stage of BC occurrence, while BC2 represents the samples at the stage of BC invasion), and the *y*-axis shows the standardized relative abundance of lipids. Each cluster represents lipids with similar trends of variation, with *metabolite(s) indicating the number of lipids in each cluster. **F** Spearman correlation analysis between 9 lipid clusters and both PEA-DEBs and PEA-DEFs. Correlation strength and direction are indicated by the color of the circles in the heatmap, with blue representing negative correlations and red representing positive correlations. The size of the circles reflects the absolute value of the correlation coefficient, with larger circles indicating stronger correlations. Asterisks indicate statistical significance (*$p < 0.05$). **G** Donut plot representing the distribution of lipids included in cluster 8 across subclasses. Lipids highlighted with a red border belong to the PEA-DELs. Abbreviations: PEA, pentadecanoic acid; BC, bladder cancer; VIP, variable importance in projection; PEA-DEL, PEA-differentially enriched lipid; PEA-DEB, PEA-differentially enriched bacterium; PEA-DEF, PEA-differentially enriched fungus

To further elucidate the underlying mechanisms, we conducted proteomic analysis and found that PEA modulated key pathways involved in lipid metabolism—processes increasingly recognized as critical in cancer biology. As reported by Feng et al. [59] and Shen et al. [60], lipid metabolism not only supports tumor growth and metastasis but also shapes the tumor microenvironment. Our analysis identified apolipoproteins such as Apoe and Apob, which are enriched in cholesterol metabolism pathways and serve as central regulators of lipid metabolism, mediating cholesterol and phospholipid transport and systemic lipid availability. Apoe is primarily involved in cholesterol and phospholipid redistribution, facilitating lipid transport between tissues and modulating cellular lipid homeostasis, thereby influencing membrane composition, signaling pathways, and metabolic balance within cells [61]. Apob serves as the main structural component of low-density lipoproteins (LDL) and is essential for lipoprotein assembly and systemic lipid transport, determining the availability of lipids for energy production and membrane biosynthesis [62]. As such, dysregulation of Apoe and Apob can lead to altered lipid metabolism, and potentially impacting cellular functions relevant to cancer development, including proliferation, migration, and survival [63]. Specifically, it has been demonstrated that dysregulated lipid metabolism has been linked to BC, with elevated triglycerides and LDL, and reduced high-density lipoprotein (HDL) levels associated with increased BC risk [64]. In our study, PEA altered levels of several PEs and phosphatidylcholines (PCs), which are involved in lipid metabolism pathways, pathways related to membrane structure and signaling, autophagy, one-carbon metabolism, and cancer-related metabolic pathways involving choline and folate. These findings, in line with the work of Ping et al. [65], suggest that PEA may influence multiple aspects of BC biology by modulating membrane dynamics, lipid-mediated signaling, and metabolic reprogramming, which could in turn affect tumor proliferation, and immune regulation [66]. Autophagy plays a vital role in BC [67], as demonstrated by Li et al. [68], who found that starvation-induced autophagy enhances glycolytic activity and promotes tumor progression in BC cells. Dysregulated choline metabolism—which is essential for membrane biosynthesis and cellular signaling—has also been implicated in BC. Notably, aberrant choline metabolism is more frequently observed in advanced or invasive stages, further supporting its contribution to tumor development and progression [69, 70]. Furthermore, gut microbiome-mediated regulation of lipid metabolism has been shown to promote lipid absorption and remodeling by repressing long non-coding RNA expression [56]. In light of these findings, our study suggests that PEA may exert its anti-BC effects by modulating lipid-associated metabolic processes and pathways, potentially through interactions with gut microbiome.

The gut microbiome has been increasingly recognized for its regulatory role in host metabolism, immune function, and inflammation, all of which are key contributors to cancer development [71, 72]. In our study, PEA significantly altered the composition of gut bacterial communities at both the occurrence and invasion stages of BC. In contrast, significant changes in fungal communities were observed only during the invasion stage, suggesting that fungi may exert a more prominent influence on BC invasion than on its occurrence. This observation aligns with findings from other cancer types, such as colorectal, pancreatic, and breast cancers, where fungi have been shown to play a more pronounced role in tumor growth and immune evasion during advanced stages [73].

Specifically, PEA enhanced gut bacterial diversity and modulated the abundance of specific taxa. At the occurrence stage of BC, PEA treatment led to an increased abundance of g_*Akkermansia*, a genus within the p_*Verrucomicrobiota*, which has been implicated in promoting anti-cancer effects through modulation of the immune microenvironment [74]. Notably, s_*Akkermansia* muciniphila has been shown to enhance the efficacy of chemotherapy agents such as cisplatin by regulating host immune responses [75]. Conversely, we observed a decreased abundance of p_*Desulfobacterota* in PEA-treated groups, a phylum known for producing harmful metabolites like hydrogen sulfide, particularly g_*Desulfovibrio*, which may contribute to disease progression [76]. In terms of fungi, PEA increased the proportion of saprotrophic fungi while reduced pathogens. In ecological studies, saprotrophic fungi are known as decomposers that maintain community balance and recycle nutrients [77, 78]. While most studies on saprotrophic fungi were related with soil and environmental systems, these findings provide conceptual insight that in the gut, saprotrophic fungi may similarly contribute to maintaining a balanced mycobiome, preventing overgrowth of opportunistic pathogens, and supporting overall intestinal homeostasis [79]. By promoting these beneficial fungi and limiting pathogenic fungi, PEA may help stabilize the gut fungal community, reduce inflammation, and support overall intestinal homeostasis. In contrast, the model group was enriched in pathogenic fungi, which under dysbiotic conditions may contribute to intestinal barrier dysfunction and immune activation [80, 81]. These alterations in gut microbiome composition suggest that PEA may influence BC through microbiome modulation, exerting both protective and risk-modifying effects on host health.

In exploring the potential interplay among PEA-modulated bacteria, fungi, and host proteins, we found that Apoe and Apob were significantly correlated with PEA-affected microbial taxa. Notably, Apob showed a positive correlation with several fungi, including o_*Erysiphales*, g_*Teberdinia*, and g_*Gibberella*, indicating a possible contribution of fungal communities to lipid metabolic processes. Conversely, Apoe negatively correlated with g_*Alistipes*, a genus previously implicated in lipid metabolism regulation. This is supported by Yin et al. [82], who reported that g_*Alistipes* modulates lipid metabolism via the production of acetic acid. Additionally, Yang et al. [83] linked g_*Alistipes* enrichment to dysregulated lipid metabolism, elevated oncogenic metabolites such as lysophosphatidic acid, and compromised gut barrier integrity—factors that may contribute to cancer development. Although no significant associations between bacteria and fungi were observed overall, further studies are needed to clarify the role of their interactions in mediating PEA's effects on gut microbiome and BC.

The observed significantly correlations between specific PEs, including PE(18:0_20:1) and PE(O-18:0_20:1), and *Alistipes* taxa point toward a potential microbiome-lipid crosstalk, suggesting a mechanistic pathway through which PEA may exert its modulatory effects in BC. Consistently, together with the sCCA findings, these mediation analyses hinted at potential microbiota-lipid pathways, especially involving *Alistipes* taxa and PEs, that may partially link PEA to BC. Although the effects did not reach statistical significance, likely due to the limited sample size, these exploratory results provide a rationale for further validation in larger cohort.

Collectively, these results support a mechanistic hypothesis whereby PEA modulates *Alistipes* taxa, alters in PE(18:0_20:1) and PE(O-18:0_20:1), thereby impacting pathways, including lipid metabolism, membrane dynamics, autophagy, one-carbon metabolism, and cancer-related metabolic pathways such as choline and folate metabolism, and potentially exerting effects on BC. Future studies with larger cohorts and functional experiments are warranted to confirm causality and to explore whether targeting this microbiome-lipid interplay could offer a novel preventive or therapeutic strategy for BC.

There are several limitations that need to be acknowledged in our study. First, estimating PEA from diet is inherently prone to some unavoidable inaccuracies due to limitations of food assessment methods. Second, although promising results were observed in vitro and in vivo models, the underlying mechanisms of PEA's effects are not fully understood, and further clinical validation in humans is needed to confirm its therapeutic potential.

Conclusions

In summary, our findings suggest that PEA, through modulating lipid metabolism mediated by gut microbiome, plays a protective role in BC occurrence and invasion. By influencing key proteins involved in lipid metabolism and altering the gut microbial community, PEA appears to exert both direct and indirect effects on BC. These results highlight the complex interplay between diet, microbiome, and cancer biology, supporting the idea that dietary interventions, such as increasing PEA intake, may offer novel strategies for BC prevention and management. Further studies are needed to explore the precise mechanisms by which PEA modulates microbiome composition and function and to validate its potential as a therapeutic agent in BC care.

Abbreviations

BBN	N-butyl-N-(4-hydroxybutyl) nitrosamine
BC PEAH	High-dose PEA-treated with BBN-induced group
BC PEAL	Low-dose PEA-treated with BBN-induced group
BC	Bladder cancer
BCPP	Bladder Cancer Prognosis Programme
BMI	Body mass index
CCK-8	Cell Counting Kit-8
CIS	Carcinoma in situ
CIs	Confidence intervals
CoFID	Composition of Foods Integrated Dataset
DEF	Differentially expressed fungus
DEPs	Differentially expressed proteins
DIA-MS	Data-Independent Acquisition Mass Spectrometry
DMED	Dulbecco's modified Eagle's medium
DMSO	Dimethyl Sulfoxide
FA	Fatty acid
FBS	Fetal bovine serum
FBS	Fetal bovine serum
FDR	False discovery rate
FFQ	Food frequency questionnaire
GO	Gene Ontology
GPI	Glycosylphosphatidylinositol
H&E	Hematoxylin and eosin
ICD	International Classification of Diseases
ITS	Internal transcribed spacer
KEGG	Kyoto Encyclopedia of Genes and Genomes
LDA	Linear Discriminant Analysis
LEfSe	Linear Discriminant Analysis Effect Size
MCE	MedChemExpress
MIBC	Muscle-invasive bladder cancer
MS1	Primary Mass Spectrometry
MS2	Secondary Mass Spectrometry
NASH	Nonalcoholic steatohepatitis
NMIBC	Non-muscle-invasive bladder cancer
OCFA	Odd-chain fatty acid
OPLS-DA	Orthogonal Projections to Latent Structures-Discriminant Analysis
OR	Odds ratio
PCA	Principal component analysis
PCoA	Principal Coordinates Analysis
PE	Phosphatidylethanolamines
PEA	Pentadecanoic acid
PEA-DEB	PEA-differentially enriched bacterium
PEA-DEF	PEA-differentially enriched fungus
PEA-DELs	PEA-differentially expressed lipids
PEA-DEPs	PEA-differentially expressed proteins
PG	Phosphatidylglycerol
QC	Quality control
RPMI 1640	Roswell Park Memorial Institute 1640 Medium
sCCA	Sparse Canonical Correlation Analysis
SCFAs	Short-chain fatty acids
SD	Standard deviation
TAG	Triacylglycerols
UICC	Union for International Cancer Control
VIP	Variable Importance in Projection

Supplementary Information

The online version contains supplementary material available at https://doi.org/10.1186/s12916-025-04554-5.

Additional file 1. STROBE-checklist.

Additional file 2. Table S1 & S2; Figure S1-S10**.** Table S1: Description of food and PEA intake in the UK Biobank and the BCPP; Table S2: Baseline characteristics of the participants from the UK Biobank and the BCPP;

Figure S1: PEA inhibits the migration, invasion, and proliferation of T24 BC cells; Figure S2: GO pathway enrichment analyses of 122 unique proteins identified; Figure S3: Venn analysis between groups of gut bacteria at BC occurrence and invasion stages; Figure S4: Phylum- and genus-level of relative abundance composition of gut bacteria at BC occurrence and invasion stages; Figure S5: Phylum- and genus-level of relative abundance composition of gut fungi at BC occurrence and invasion stages; Figure S6: Functional profiling of PEA-DEFs based on FUNGuild analysis; Figure S7: Relative abundance composition of fecal lipid species in the samples at BC occurrence and invasion stages; Figure S8: Principal component analysis (PCA) of fecal lipidomics in different groups; Figure S9: Sparse Canonical Correlation Analysis (sCCA) of PEA-DELs, PEA-DEBs, and PEA-DEFs; Figure S10: Spearman correlation analysis between 11 PEA-DELs and PEA-DEPs.

Additional file 3. ARRIVE-checklist.

Additional file 4. Table S3 & S15**.** Table S3: Differential analysis on serum proteomics between BC model and PEA-treated groups (i.e., BC PEAL and BC PEAH) at both occurrence and invasion stages respectively; Table S4: LEfSe on fecal bacteria between BC model and PEA-treated groups (i.e., BC PEAL and BC PEAH) at both occurrence and invasion stages respectively; Table S5: LEfSe on fecal fungi between BC model and PEA-treated groups (i.e., BC PEAL and BC PEAH) at both occurrence and invasion stages respectively; Table S6: Functional profiling of PEA-DEFs using FUNGuild; Table S7: Spearman correlation between PEA-DEPs and PEA-DEBs, and between PEA-DEPs and PEA-DEFs; Table S8: Spearman correlation between PEA-DEBs and PEA-DEFs; Table S9: Differential lipid analysis between BC model and PEA-treated groups (i.e., BC PEAL and BC PEAH); Table S10: Pathway-level lipid metabolism analysis based on Lipid Ontology and KEGG pathways; Table S11: Spearman correlation between PEA-DELs and PEA-DEBs, and between PEA-DELs and PEA-DEFs; Table S12: K-Means clustering analysis of differential lipid abundance in different groups; Table S13: Spearman correlation between lipid clusters and PEA-DEBs, and between lipid clusters and PEA-DEFs; Table S14: Mediation analysis of PEA effects on BC via microbiota and lipidomic; Table S15: Spearman correlation between PEA-DELs and PEA-DEPs.

Acknowledgements
We thank the staff at EVLiXiR Biotech (Nanjing, China), Shanghai Biotree Biotech Co., Ltd. and Nanjing jiangbei New Area biopharmaceutical Public service Platform Co., Ltd. for data generation and processing.

Artificial intelligence disclosure

No generative artificial intelligence (AI) tools were used in the writing, editing, data analysis, or figure preparation of this manuscript.

Authors' contributions

EYW.Y, H.X, and LM.C conceived the study concept and design. YT.C and Y.Y analysed the data. YT.C, J.S, Y.Y, and H.Z contributed to the fieldwork, data collection, and data curation. YT.C contributed to the visualization of the data. EYW.Y and YT.C wrote the first draft of the manuscript. J.S, Y.Y, H.Z, A.W, Y.S, QR.Q, GJ.S, SK.W, XD.W, SJ.W, WC.L, KK.C, N.D.J, RT.B, MP.Z, LM.C, and H.X, contributed to the critical revision of the manuscript. YT.C, J.S, Y.Y, and H.Z contributed equally to the work. EYW.Y is the guarantor of this work and, as such, had full access to all of the data in the study and took responsibility for the integrity of the data and the accuracy of the data analysis. All authors read and approved the final manuscript.

Funding
This study was supported by: the National Natural Science Foundation of China (NSFC, 82574191; 82204033); the Natural Science Foundation of Jiangsu Province (BK20220826); the Jiangsu Provincial Double-Innovation Doctor Program (SSCBS20220169); Fundamental Research Funds for the Central Universities of China (2242022R10062/3225002202A1); Medical Foundation of Southeast University (4060692202/021); Zhishan Young Scholar Award at the Southeast University (2242023R40031); The Scientific Research Project for Health Commission of Anhui Province (AHWJ2023A20172; AHWJ2023BAa20055); Natural Science Research Project of Anhui Educational Committee (2024AH050663). The funders had no role in the study design, data collection, decision to publish, or preparation of the manuscript.

Data availability

The Mass Spectrometry raw data of proteomics have been deposited to the ProteomeXchange Consortium via the iProX repository and can be accessed at https://www.iprox.cn/page/project.html?id=IPX0011653000. The raw sequence data for gut microbiome have been deposited in the Genome Sequence Archive, with 16S rRNA data for bacterial communities available under accession number GRA033961 (https://ngdc.cncb.ac.cn/gsa/browse/CRA033961) and ITS data for fungal communities available under GRA033963 (https://ngdc.cncb.ac.cn/gsa/browse/CRA033963). For the UK Biobank, the data are available at UK Biobank website: https://www.ukbiobank.ac.uk/. Data access is available through applications. This research was conducted using the application #55889. For the BCPP, the data are available at BCPP website: http:/www.bcpp.bham.ac.uk. BCPP data and access to specimens stored within the BCPP tissue bank will be made available to qualified research groups, subject to ethical approval and permission from the BCPP Working Group. Requests should be submitted to the BCPP Study Office following the procedures outlined on the BCPP website. The key codes for analysis in this study are available at GitHub (https://github.com/TeamEYu/PEA_BC) via reasonable request from the corresponding author.

Declarations

Ethics approval and consent to participate

The studies involving human participants were reviewed and approved by NHS National Research Ethics Service North West (11/NW/0382) and Nottingham Multi-center Research Ethics Committee (06/MRE04/65), and written informed consent was obtained from all participants. All experimental procedures were conducted in compliance with the institutional guidelines for the care and use of laboratory animals in China and approved by the Animal Ethical Council of Southeast University. Animal welfare and experimental protocols were strictly in accordance with the guidelines for the care and use of laboratory animals.

Consent for publication

Not applicable.

Competing interests

The authors declare no competing interests.

Author details
[1]Key Laboratory of Environmental Medicine and Engineering of Ministry of Education, School of Public Health, Southeast University, Nanjing 210009, China. [2]Department of Epidemiology & Biostatistics, School of Public Health, Southeast University, Nanjing 210009, China. [3]Research Institute for Environment and Health, Nanjing University of Information Science and Technology, Nanjing 210044, China. [4]Department of Nutrition and Food Hygiene, School of Public Health, Southeast University, Nanjing 210009, China. [5]Department of Critical Care Medicine, Jinling Hospital, Medical School of Nanjing University, Nanjing 210002, China. [6]Department of Epidemiology, School of Nutrition and Translational Research in Metabolism, Maastricht University, Maastricht 6229ER, The Netherlands. [7]Department of Gastroenterology, Ma'anshan People's Hospital, Ma'anshan 243000, China. [8]Ma'anshan Center for Disease Control and Prevention, Ma'anshan 243000, China. [9]The Affiliated Ma'anshan Center for Disease Control and Prevention of Anhui Medical University, Ma'anshan, 243000, China. [10]Department of Epidemiology and Biostatistics, School of Public Health, Anhui Medical University, Hefei 230032, China. [11]Nutrition and Cancer Biology Laboratory, Jean Mayer USDA Human Nutrition Research Center On Aging at Tufts University, Boston, MA 02111, USA. [12]Gerald J. and Dorothy R. Friedman School of Nutrition Science and Policy, Tufts University, Boston, MA 02111, USA. [13]Center for Obesity and Metabolic Diseases Research, School of Basic Medicine, The First Affiliated Hospital of Chongqing Medical University, Chongqing Medical University, Chongqing, China. [14]Department of Urology, Affiliated Zhongda Hospital of Southeast University, Nanjing 210009, China. [15]Department of Applied Health Research, University of Birmingham, Birmingham B152TT, UK. [16]Bladder Cancer Research Centre, College of Medicine and Health, University of Birmingham, Birmingham B152TT, UK. [17]Institute of Cancer Research, London SW7 3RP, UK. [18]Changzhou Medical Center, The Third Affiliated Hospital of Nanjing Medical University, Nanjing Medical University, Changzhou 213003, China.

[19]Department of Cardiology, The First Affiliated Hospital with Nanjing Medical University, Nanjing Medical University, Nanjing 210029, China.

Received: 18 June 2025 Accepted: 26 November 2025

References

1. Venn-Watson S, Lumpkin R, Dennis EA. Efficacy of dietary odd-chain saturated fatty acid pentadecanoic acid parallels broad associated health benefits in humans: could it be essential? Sci Rep. 2020;10(1):8161.
2. O'Donnell-Megaro AM, Barbano DM, Bauman DE. Survey of the fatty acid composition of retail milk in the United States including regional and seasonal variations. J Dairy Sci. 2011;94(1):59–65.
3. Risérus U, Marklund M. Milk fat biomarkers and cardiometabolic disease. Curr Opin Lipidol. 2017;28(1):46–51.
4. Chooi YC, Zhang QA, Magkos F, Ng M, Michael N, Wu X, et al. Effect of an Asian-adapted Mediterranean diet and pentadecanoic acid on fatty liver disease: the TANGO randomized controlled trial. Am J Clin Nutr. 2024;119(3):788–99.
5. Singh D, Mehghini P, Rodriguez-Palacios A, Di Martino L, Cominelli F, Basson AR. Anti-inflammatory effect of dietary pentadecanoic fatty acid supplementation on inflammatory bowel disease in SAMP1/YitFc mice. Nutrients. 2024. https://doi.org/10.3390/nu16173031.
6. Forouhi NG, Koulman A, Sharp SJ, Imamura F, Kröger J, Schulze MB, et al. Differences in the prospective association between individual plasma phospholipid saturated fatty acids and incident type 2 diabetes: the EPIC-InterAct case-cohort study. Lancet Diabetes Endocrinol. 2014;2(10):810–8.
7. Imamura F, Fretts A, Marklund M, Ardisson Korat AV, Yang WS, Lankinen M, et al. Fatty acid biomarkers of dairy fat consumption and incidence of type 2 diabetes: A pooled analysis of prospective cohort studies. PLoS Med. 2018;15(10):e1002670.
8. Santaren ID, Watkins SM, Liese AD, Wagenknecht LE, Rewers MJ, Haffner SM, et al. Serum pentadecanoic acid (15:0), a short-term marker of dairy food intake, is inversely associated with incident type 2 diabetes and its underlying disorders. Am J Clin Nutr. 2014;100(6):1532–40.
9. Biong AS, Veierød MB, Ringstad J, Thelle DS, Pedersen JI. Intake of milk fat, reflected in adipose tissue fatty acids and risk of myocardial infarction: a case-control study. Eur J Clin Nutr. 2006;60(2):236–44.
10. Djousse L, Biggs ML, Matthan NR, Ix JH, Fitzpatrick AL, King I, et al. Serum individual nonesterified fatty acids and risk of heart failure in older adults. Cardiology. 2021;146(3):351–8.
11. Khaw KT, Friesen MD, Riboli E, Luben R, Wareham N. Plasma phospholipid fatty acid concentration and incident coronary heart disease in men and women: the EPIC-Norfolk prospective study. PLoS Med. 2012;9(7):e1001255.
12. Liang J, Zhou Q, Kwame Amakye W, Su Y, Zhang Z. Biomarkers of dairy fat intake and risk of cardiovascular disease: a systematic review and meta analysis of prospective studies. Crit Rev Food Sci Nutr. 2018;58(7):1122–30.
13. Kratz M, Marcovina S, Nelson JE, Yeh MM, Kowdley KV, Callahan HS, et al. Dairy fat intake is associated with glucose tolerance, hepatic and systemic insulin sensitivity, and liver fat but not β-cell function in humans. Am J Clin Nutr. 2014;99(6):1385–96.
14. Sawh MC, Wallace M, Shapiro E, Goyal NP, Newton KP, Yu EL, et al. Dairy Fat Intake, Plasma Pentadecanoic Acid, and Plasma Iso-heptadecanoic Acid Are Inversely Associated With Liver Fat in Children. J Pediatr Gastroenterol Nutr. 2021;72(4):e90–6.
15. Wei W, Wong CC, Jia Z, Liu W, Liu C, Ji F, et al. *Parabacteroides distasonis* uses dietary inulin to suppress NASH via its metabolite pentadecanoic acid. Nat Microbiol. 2023;8(8):1534–48.
16. Ghamarzad Shishavan N, Masoudi S, Mohamadkhani A, Sepanlou SG, Sharafkhah M, Poustchi H, et al. Dietary intake of fatty acids and risk of pancreatic cancer: Golestan cohort study. Nutr J. 2021;20(1):69.
17. Jiang Y, Li LT, Hou SH, Chen LN, Zhang CX. Association between dietary intake of saturated fatty acid subgroups and breast cancer risk. Food Funct. 2024;15(4):2282–94.
18. Teng C, Ren R, Liu Z, Wang J, Shi S, Kang YE, et al. C15:0 and C17:0 partially mediate the association of milk and dairy products with bladder cancer risk. J Dairy Sci. 2024;107(5):2586–605.
19. Venn-Watson S, Schork NJ. Pentadecanoic acid (C15:0), an essential fatty acid, shares clinically relevant cell-based activities with leading longevity-enhancing compounds. Nutrients. 2023. https://doi.org/10.3390/nu15214607.
20. Pelucchi C, Bosetti C, Negri E, Malvezzi M, La Vecchia C. Mechanisms of disease: the epidemiology of bladder cancer. Nat Clin Pract Urol. 2006;3(6):327–40.
21. Yu EY, Zhang H, Fu Y, Chen YT, Tang QY, Liu YX, et al. Integrative Multi-Omics Analysis for the Determination of Non-Muscle Invasive vs. Muscle Invasive Bladder Cancer: A Pilot Study. Curr Oncol. 2022;29(8):5442–56.
22. Fu WC, Li HY, Li TT, Yang K, Chen JX, Wang SJ, et al. Pentadecanoic acid promotes basal and insulin-stimulated glucose uptake in C2C12 myotubes. Food Nutr Res. 2021;65:4527. https://doi.org/10.29219/fnr.v65.4527.
23. To NB, Truong VN, Ediriweera MK, Cho SK. Effects of combined pentadecanoic acid and tamoxifen treatment on tamoxifen resistance in MCF-7/SC breast cancer cells. Int J Mol Sci. 2022. https://doi.org/10.3390/ijms231911340.
24. To NB, Nguyen YT, Moon JY, Ediriweera MK, Cho SK. Pentadecanoic acid, an odd-chain fatty acid, suppresses the stemness of MCF-7/SC human breast cancer stem-like cells through JAK2/STAT3 signaling. Nutrients. 2020. https://doi.org/10.3390/nu12061663.
25. Ediriweera MK, To NB, Lim Y, Cho SK. Odd-chain fatty acids as novel histone deacetylase 6 (HDAC6) inhibitors. Biochimie. 2021;186:147–56.
26. Venn-Watson SK, Butterworth CN. Broader and safer clinically-relevant activities of pentadecanoic acid compared to omega-3: evaluation of an emerging essential fatty acid across twelve primary human cell-based disease systems. PLoS ONE. 2022;17(5):e0268778.
27. Wang J, Zheng S, Li Z, Tang Y, Huang Y, Wang J, et al. Pentadecanoic acid (C15:0, PA) induces mild maternal glucose intolerance and promotes the growth of the offspring partly through up-regulating liver PPARα and MAPK signaling pathways. Food Funct. 2024;15(23):11400–14.
28. Galdiero E, Ricciardelli A, D'Angelo C, de Alteriis E, Maione A, Albarano L, et al. Pentadecanoic acid against *Candida albicans-Klebsiella pneumoniae* biofilm: towards the development of an anti-biofilm coating to prevent polymicrobial infections. Res Microbiol. 2021;172(7–8):103880.
29. Ricciardelli A, Casillo A, Corsaro MM, Tutino ML, Parrilli E, van der Mei HC. Pentadecanal and pentadecanoic acid coatings reduce biofilm formation of *Staphylococcus epidermidis* on PDMS. Pathog Dis. 2020. https://doi.org/10.1093/femspd/ftaa012.
30. Eckburg PB, Bik EM, Bernstein CN, Purdom E, Dethlefsen L, Sargent M, et al. Diversity of the human intestinal microbial flora. Science. 2005;308(5728):1635–8.
31. Fan L, Xia Y, Wang Y, Han D, Liu Y, Li J, et al. Gut microbiota bridges dietary nutrients and host immunity. Sci China Life Sci. 2023;66(11):2466–514.
32. Saftien A, Puschhof J, Elinav E. Fungi and cancer. Gut. 2023;72(7):1410–25.
33. Zhou X, Chen X, Davis MM, Snyder MP. Embracing interpersonal variability of microbiome in precision medicine. Phenomics. 2025. https://doi.org/10.1007/s43657-024-00201-w.
34. Xiao W, Chen Q, Liu C, Yu Y, Liu T, Jin Y, et al. Gut microbiota in cancer: From molecular mechanisms to precision medicine applications. iMeta. 2025;4(2):e70017. https://doi.org/10.1002/imt2.70017.
35. Salazar AM, Neugent ML, De Nisco NJ, Mysorekar IU. Gut-bladder axis enters the stage: implication for recurrent urinary tract infections. Cell Host Microbe. 2022;30(8):1066–9.
36. Sudlow C, Gallacher J, Allen N, Beral V, Burton P, Danesh J, et al. UK biobank: an open access resource for identifying the causes of a wide range of complex diseases of middle and old age. PLoS Med. 2015;12(3):e1001779.
37. Zeegers MP, Bryan RT, Langford C, Billingham L, Murray P, Deshmukh NS, et al. The West Midlands Bladder Cancer Prognosis Programme: rationale and design. BJU Int. 2010;105(6):784–8.
38. Dąbrowski G, Konopka I. Update on food sources and biological activity of odd-chain, branched and cyclic fatty acids—A review. Trends Food Sci Technol. 2022;119:514–29.
39. Mills A, Patel S, Crawley H. Great Britain Ministry of Agriculture, Fisheries and Food. *Food Portion Size*. 2nd ed. London: H.M.S.O.; 1993.
40. Finglas PM, Roe M, Pinchen H, et al. McCance and Widdowson's The Composition of Foods Integrated Dataset. Cambridge: Royal Society of Chemistry; 2021.

41. Gao F, Zhou C, Qiu W, Wu H, Li J, Peng J, et al. Total flavonoids from Semen Cuscutae target MMP9 and promote invasion of EVT cells via Notch/AKT/MAPK signaling pathways. Sci Rep. 2018;8(1):17342.
42. Wang X, Ning Y, Li C, Gong Y, Huang R, Hu M, et al. Alterations in the gut microbiota and metabolite profiles of patients with Kashin-Beck disease, an endemic osteoarthritis in China. Cell Death Dis. 2021;12(11):1015.
43. Zhao C, An X, Xiao L, Chen J, Huang D, Chen L, et al. Integrative multi-omics analysis reveals molecular signatures of central obesity in children. Pediatr Res. 2025. https://doi.org/10.1038/s41390-025-03958-6.
44. Nguyen NH, Song Z, Bates ST, Branco S, Tedersoo L, Menke J, et al. FUNGuild: an open annotation tool for parsing fungal community datasets by ecological guild. Fungal Ecol. 2016;20:241–8.
45. Li H, Zhang S, Chen L, Pan X, Li Z, Huang T, et al. Identifying functions of proteins in mice with functional embedding features. Front Genet. 2022;13:909040.
46. Ansa-Addo EA, Huang HC, Riesenberg B, Iamsawat S, Borucki D, Nelson MH, et al. RNA binding protein PCBP1 is an intracellular immune checkpoint for shaping T cell responses in cancer immunity. Sci Adv. 2020;6(22):eaaz3865.
47. Hockla A, Miller E, Salameh MA, Copland JA, Radisky DC, Radisky ES. PRSS3/mesotrypsin is a therapeutic target for metastatic prostate cancer. Mol Cancer Res. 2012;10(12):1555–66.
48. Jiang G, Cao F, Ren G, Gao D, Bhakta V, Zhang Y, et al. PRSS3 promotes tumour growth and metastasis of human pancreatic cancer. Gut. 2010;59(11):1535–44.
49. Ma R, Ye X, Cheng H, Ma Y, Cui H, Chang X. *PRSS3* expression is associated with tumor progression and poor prognosis in epithelial ovarian cancer. Gynecol Oncol. 2015;137(3):546–52.
50. Fu Y, Zou T, Shen X, Nelson PJ, Li J, Wu C, et al. Lipid metabolism in cancer progression and therapeutic strategies. MedComm. 2021;2(1):27–59.
51. Nirgude S, Choudhary B. Insights into the role of GPX3, a highly efficient plasma antioxidant, in cancer. Biochem Pharmacol. 2021;184:114365.
52. Huang H, Tang Q, Li S, Qin Y, Zhu G. TGFBI: a novel therapeutic target for cancer. Int Immunopharmacol. 2024;134:112180.
53. Kriaa A, Bourgin M, Potiron A, Mkaouar H, Jablaoui A, Gérard P, et al. Microbial impact on cholesterol and bile acid metabolism: current status and future prospects. J Lipid Res. 2019;60(2):323–32.
54. Hays KE, Pfaffinger JM, Ryznar R. The interplay between gut microbiota, short-chain fatty acids, and implications for host health and disease. Gut Microbes. 2024;16(1):2393270.
55. Lin R, Liu W, Piao M, Zhu H. A review of the relationship between the gut microbiota and amino acid metabolism. Amino Acids. 2017;49(12):2083–90.
56. Wang Y, Wang M, Chen J, Li Y, Kuang Z, Dende C, et al. The gut microbiota reprograms intestinal lipid metabolism through long noncoding RNA Snhg9. Science. 2023;381(6660):851–7.
57. Nüse B, Holland T, Rauh M, Gerlach RG, Mattner J. L-arginine metabolism as pivotal interface of mutual host-microbe interactions in the gut. Gut Microbes. 2023;15(1):2222961.
58. Fu Y, Gou W, Zhong H, Tian Y, Zhao H, Liang X, et al. Diet-gut microbiome interaction and its impact on host blood glucose homeostasis: a series of nutritional n-of-1 trials. EBioMedicine. 2025;111:105483.
59. Feng F, Pan L, Wu J, Li L, Xu H, Yang L, et al. Cepharanthine inhibits hepatocellular carcinoma cell growth and proliferation by regulating amino acid metabolism and suppresses tumorigenesis in vivo. Int J Biol Sci. 2021;17(15):4340–52.
60. Shen X, Hu B, Xu J, Qin W, Fu Y, Wang S, et al. The m6A methylation landscape stratifies hepatocellular carcinoma into 3 subtypes with distinct metabolic characteristics. Cancer Biol Med. 2020;17(4):937–52.
61. Mahley RW, Rall SC Jr. Apolipoprotein E: far more than a lipid transport protein. Annu Rev Genomics Hum Genet. 2000;1:507–37.
62. Rauscher FG, Wang M, Francke M, Wirkner K, Tönjes A, Engel C, et al. Renal function and lipid metabolism are major predictors of circumpapillary retinal nerve fiber layer thickness-the LIFE-Adult Study. BMC Med. 2021;19(1):202.
63. Ren L, Yi J, Li W, Zheng X, Liu J, Wang J, et al. Apolipoproteins and cancer. Cancer Med. 2019;8(16):7032–43.
64. Xi Y, Yang Y, Wang Z, Wang J. Higher genetically predicted triglyceride level increases the bladder cancer risk independent of LDL and HDL levels. Sci Rep. 2024;14(1):18652.
65. Ping Y, Shan J, Qin H, Li F, Qu J, Guo R, et al. PD-1 signaling limits expression of phospholipid phosphatase 1 and promotes intratumoral CD8(+) T cell ferroptosis. Immunity. 2024;57(9):2122-39.e9.
66. Yang YY, Hong SY, Xun Y, Liu CQ, Sun JX, Xu JZ, et al. Characterization of the lipid metabolism in bladder cancer to guide clinical therapy. J Oncol. 2022;2022:7679652.
67. Li F, Guo H, Yang Y, Feng M, Liu B, Ren X, et al. Autophagy modulation in bladder cancer development and treatment (Review). Oncol Rep. 2019;42(5):1647–55.
68. Li T, Tong H, Yin H, Luo Y, Zhu J, Qin Z, et al. Starvation induced autophagy promotes the progression of bladder cancer by LDHA mediated metabolic reprogramming. Cancer Cell Int. 2021;21(1):597.
69. Han Z, Gu J, Xin J, Liu H, Wu Y, Du M, et al. Genetic variants in choline metabolism pathway are associated with the risk of bladder cancer in the Chinese population. Arch Toxicol. 2022;96(6):1729–37.
70. Loras A, Suárez-Cabrera C, Martínez-Bisbal MC, Quintás G, Paramio JM, Martínez-Máñez R, et al. Integrative metabolomic and transcriptomic analysis for the study of bladder cancer. Cancers. 2019;11(5):686.
71. Browne HP, Neville BA, Forster SC, Lawley TD. Transmission of the gut microbiota: spreading of health. Nat Rev Microbiol. 2017;15(9):531–43.
72. Vaitkute G, Panic G, Alber DG, Faizura-Yeop I, Cloutman-Green E, Swann J, et al. Linking gastrointestinal microbiota and metabolome dynamics to clinical outcomes in paediatric haematopoietic stem cell transplantation. Microbiome. 2022;10(1):89.
73. Bilal H, Khan MN, Khan S, Shafiq M, Fang W, Zeng Y, et al. Fungal Influences on Cancer Initiation, Progression, and Response to Treatment. Cancer Res. 2025;85(3):413–23.
74. Li J, Lin S, Vanhoutte PM, Woo CW, Xu A. *Akkermansia muciniphila* protects against atherosclerosis by preventing metabolic endotoxemia-induced inflammation in *Apoe-/-* mice. Circulation. 2016;133(24):2434–46.
75. Chen Z, Qian X, Chen S, Fu X, Ma G, Zhang A. *Akkermansia muciniphila* enhances the antitumor effect of Cisplatin in Lewis lung cancer mice. J Immunol Res. 2020;2020:2969287.
76. Zhou H, Huang D, Sun Z, Chen X. Effects of intestinal *Desulfovibrio* bacteria on host health and its potential regulatory strategies: a review. Microbiol Res. 2024;284:127725.
77. Frąc M, Hannula SE, Bełka M, Jędryczka M. Fungal biodiversity and their role in soil health. Front Microbiol. 2018;9:707.
78. Crowther TW, Boddy L, Hefin Jones T. Functional and ecological consequences of saprotrophic fungus-grazer interactions. ISME J. 2012;6(11):1992–2001.
79. van der Wal A, Geydan TD, Kuyper TW, de Boer W. A thready affair: linking fungal diversity and community dynamics to terrestrial decomposition processes. FEMS Microbiol Rev. 2013;37(4):477–94.
80. Huang Y, Wang Y, Huang X, Yu X. Unveiling the overlooked fungi: the vital of gut fungi in inflammatory bowel disease and colorectal cancer. Gut Pathog. 2024;16(1):59.
81. Ho J, Camilli G, Griffiths JS, Richardson JP, Kichik N, Naglik JR. *Candida albicans* and candidalysin in inflammatory disorders and cancer. Immunology. 2021;162(1):11–6.
82. Yin J, Li Y, Han H, Chen S, Gao J, Liu G, et al. Melatonin reprogramming of gut microbiota improves lipid dysmetabolism in high-fat diet-fed mice. J Pineal Res. 2018;65(4):e12524.
83. Yang J, Wei H, Zhou Y, Szeto CH, Li C, Lin Y, et al. High-Fat Diet Promotes Colorectal Tumorigenesis Through Modulating Gut Microbiota and Metabolites. Gastroenterology. 2022;162(1):135-49.e2.

Publisher's Note